Tectonics®

RESEARCH ARTICLE
10.1029/2022TC007524

Volcano-Tectonic Evolution of the Christiana-Santorini-Kolumbo Rift Zone

J. Preine[1], C. Hübscher[1], J. Karstens[2], and P. Nomikou[3]

[1]University of Hamburg, Institute of Geophysics, Hamburg, Germany, [2]GEOMAR – Helmholtz Zentrum für Ozeanforschung, Marine Geophysics, Kiel, Germany, [3]National and Kapodistrian University of Athens, Athens, Greece

Abstract Located on the Hellenic Arc, the Christiana-Santorini-Kolumbo (CSK) rift zone represents one of the most active and hazardous volcano-tectonic systems in the Mediterranean. Although this rift zone has been intensively studied, its tectonic evolution and the interplay of volcanism and tectonism are still poorly understood. In this study, we use high-resolution reflection seismic imagery to reconstruct the opening of the rift basins. For the first time, we relate the activity of individual faults with the activity of specific volcanic centers in space and time. Our analysis shows a pre-volcanic NNE-SSW-oriented paleo basin underneath the CSK volcanoes, representing a transfer zone between Pliocene ESE-WNW-oriented basins, which was overprinted by a NE-SW-oriented tectonic regime hosting Late Pliocene volcanism that initiated at the Christiana Volcano. All subsequent volcanoes evolved parallel to this trend. Two major Pleistocene tectonic pulses preceded fundamental changes in the volcanism of the CSK rift including the occurrence of widespread small-scale volcanic centers followed by focusing of activity at Santorini with increasing explosivity. The observed correlation between changes in the tectonic system and the magmatism of the CSK volcanoes suggests a deep-seated tectonic control of the volcanic plumbing system. In turn, our analysis reveals the absence of large-scale faults in basin segments affected by volcanism indicating a secondary feedback mechanism on the tectonic system. A comparison with the evolution of the neighboring Kos-Nisyros-Yali volcanic field zone and Rhodos highlights concurrent regional volcano-tectonic changes, suggesting a potential arc-wide scale of the observed volcano-tectonic interplay.

Plain Language Summary How do regional tectonic movements and large volcanoes interact? Seismological studies indicate complex volcano-tectonic feedback links, but, so far, information on the long-term interactions between tectonics and volcanism is rarely available. The Christiana-Santorini-Kolumbo (CSK) rift zone lies in the Aegean Sea and is notorious for its devastating volcanic eruptions, earthquakes, and tsunamis. This region offers the opportunity to study volcano-tectonic interactions over several million years. In this study, we use high-resolution seismic imagery to reconstruct the evolution of the rift basins and the CSK volcanoes. We find that all volcanoes lie in a Pliocene transfer zone connecting extensional basins. Volcanism initiated as this older tectonic regime was intersected by a NE-SW-directed fault system. Subsequently, all volcanoes evolved parallel to this trend. Several distinct tectonic reorganizations occurred in the Pleistocene, which had a pronounced influence on the CSK volcanoes. In turn, our analysis indicates that the emergence of volcanism also impacted the tectonic evolution of the rift system hindering the evolution of large-scale normal faults in the volcanic basins. The observed tectonic reorganizations seem to reflect major changes in the stress regime of the Hellenic Arc, potentially also affecting adjacent volcanic centers whose volcano-tectonic evolution is only poorly constrained so far.

Key Points:

- We reconstruct the volcano-tectonic evolution of the Christiana-Santorini-Kolumbo rift zone using multichannel seismic data
- The overprint of a Pleistocene NE-SW striking fault system on a Pliocene E-W oriented system initiated the emergence of volcanism
- Regional tectonics had a primary control on the volcanic plumbing system, while magmatism had a secondary influence on the tectonic system

Supporting Information:

Supporting Information may be found in the online version of this article.

Correspondence to:

J. Preine,
jonas.preine@uni-hamburg.de

Citation:

Preine, J., Hübscher, C., Karstens, J., & Nomikou, P. (2022). Volcano-tectonic evolution of the Christiana-Santorini-Kolumbo rift zone. *Tectonics*, *41*, e2022TC007524. https://doi.org/10.1029/2022TC007524

Received 9 AUG 2022
Accepted 7 NOV 2022

Author Contributions:

Conceptualization: J. Preine, C. Hübscher, J. Karstens
Data curation: J. Preine, J. Karstens
Formal analysis: J. Preine
Funding acquisition: C. Hübscher
Investigation: J. Preine, C. Hübscher, J. Karstens, P. Nomikou
Methodology: J. Preine, C. Hübscher
Project Administration: C. Hübscher, J. Karstens, P. Nomikou
Resources: C. Hübscher
Supervision: C. Hübscher
Visualization: J. Preine, J. Karstens
Writing – original draft: J. Preine

1. Introduction

The interplay of volcanism and tectonism has shaped many volcanic systems across the world (Acocella, 2021). Regional tectonics weakens the crust through increased faulting and fracturing creating pathways for magmatic fluids to ascend to the surface, although the controlling mechanisms remain elusive (e.g., Hill et al., 2002; Manga & Brodsky, 2006). Our current knowledge of volcano-tectonic feedback mechanisms is based mostly on the interplay of earthquakes and volcanic eruptions on time scales ranging from minutes to decades by direct observations or historic records (e.g., Manga & Brodsky, 2006; Watt et al., 2009). These studies revealed that tectonic movements can change stress levels in the crust and the underlying mantle, influencing production and ascent rates, as well as sizes and explosivities of eruptions. In turn, volcanism can alter the stress of the crust by accommodating extensional strain and inhibiting the formation of faults (Faulds & Varga, 1998) highlighting complex feedback

Writing – review & editing: C. Hübscher, J. Karstens, P. Nomikou

mechanisms between tectonics and volcanism that involve a competition between magmatic and tectonic strain accommodation (e.g., Acocella & Trippanera, 2016; Keir et al., 2006; Wilson et al., 2019). However, the dynamics of long-term interactions (>100 ka) between tectonics and magmatism are less well understood, since they require knowledge of the past dynamics of the tectonic stress field and the volcanic behavior, which are rarely available (Giba et al., 2013). Therefore, our current knowledge about the influence of regional, long-term tectonic stress regimes on volcanic plumbing systems and vice versa remains immature.

Located on the Hellenic Volcanic Arc in the southern Aegean Sea (Figure 1a), the Christiana-Santorini-Kolumbo (CSK) volcanic field (Figure 1c) offers the opportunity to study the interaction of a back-arc rift zone and its volcanic plumbing system over the course of more than 2 million years (Piper et al., 2007; Preine, Karstens, Hübscher, Nomikou, et al., 2022). Here, the history of volcanism and rift evolution is recorded in the sedimentary basins, which have been the target of numerous geophysical surveys in recent decades. These studies analyzed the seafloor morphology of the area (e.g., Hooft et al., 2017; Nomikou, Hübscher, et al., 2018) as well as the upper crustal structure of the rift zone (Heath et al., 2019, 2021; Hooft et al., 2019; McVey et al., 2020; Schmid et al., 2022), the seismostratigraphy of the rift basins (e.g., Hübscher et al., 2015; Nomikou, Hübscher, et al., 2016; Nomikou, Hübscher, et al., 2018; Nomikou et al., 2019; Preine, Karstens, Hübscher, Crutchley, et al., 2022), and the spatio-temporal evolution of the CSK volcanic centers (Figure 1b) (e.g., Hübscher et al., 2015; Preine, Karstens, Hübscher, Nomikou, et al., 2022). However, until now, reconstructions of the tectonic evolution of the rift basins have been lacking, which are crucial to identifying volcano-tectonic feedback mechanisms at the CSK rift zone. Understanding these interactions is critical to enable an accurate hazard assessment for the eastern Mediterranean to which the CSK field poses a major threat having produced devastating events such as the iconic Minoan eruption approx. 3,600 years ago (Druitt et al., 2019; Johnston et al., 2014; Nomikou, Druitt, et al., 2016) or the tsunamigenic 1956 magnitude 7.4 Amorgos earthquake (Figure 1c) (Brüstle et al., 2014; Nomikou, Hübscher, et al., 2018).

In this study, we utilize an extensive collection of high-resolution reflection seismic data to map the distribution of seismostratigraphic units and the activity of faults throughout the entire CSK rift zone. In addition, we use horizon flattening to reconstruct the evolution of individual basins. Our objectives are to (a) reconstruct the tectonic evolution of specific rift basins, (b) relate the tectonic evolution of the rift system to the volcanic evolution of the CSK centers, (c) investigate volcano-tectonic feedback mechanisms, and (d) link these findings to the large-scale evolution of the eastern Hellenic Arc.

2. Geological Framework

2.1. Tectonic Background

The Hellenic Arc in the southern Aegean Sea represents the seismically and volcanically most active region in the Mediterranean Sea (Figure 1a) (Bohnhoff et al., 2006). Formed as the consequence of the subduction of the African plate beneath the Eurasian plate, the Hellenic Arc is an arcuate belt reaching from the Adriatic Sea towards western Anatolia, where it transitions into the Cyprus arc (Figure 1a) (e.g., Le Pichon & Angelier, 1979; Royden & Papanikolaou, 2011). Since the Late Miocene, the Hellenic Arc has stepped southwards and increased in curvature, leading to enhanced extension and intensive internal deformation of the Aegean microplate (e.g., ten Veen & Kleinspehn, 2002). These processes have been attributed to the rollback of the subducted African slab induced by the downwards pull of the subducted African slab (e.g., Le Pichon & Angelier, 1979; Le Pichon & Kreemer, 2010), gravitational forcing associated with overthickened Alpine crust (e.g., Jolivet, 2001), and westward movement of the Anatolian plate (Le Pichon & Kreemer, 2010; Taymaz et al., 1991). The interplay of these processes produced the complex neotectonic horst and graben structures of the Cycladic islands (Le Pichon & Kreemer, 2010; Royden & Papanikolaou, 2011), where crustal thicknesses range from 20 to 30 km, compared to 40–50 km under mainland Greece and Turkey (Zhu et al., 2006).

The Aegean crust consists of metamorphic rocks belonging to the Attico-Cycladic complex, formed as a result of compressional orogeny in the early Cenozoic (Piper et al., 2007). During Miocene to Pliocene, N-S-directed extension led to basin subsidence in the southern Aegean forming multiple basins bounded by E-W-directed listric normal faults (Anastasakis & Piper, 2005; Piper et al., 2007). Increasing curvature of the Hellenic Arc led to counterclockwise rotation of the eastern segments of the Aegean in the Pliocene and Pleistocene, e.g. at Rhodos (Figure 1a) (Van Hinsbergen et al., 2007). This was accommodated by major arc-normal and arc-parallel

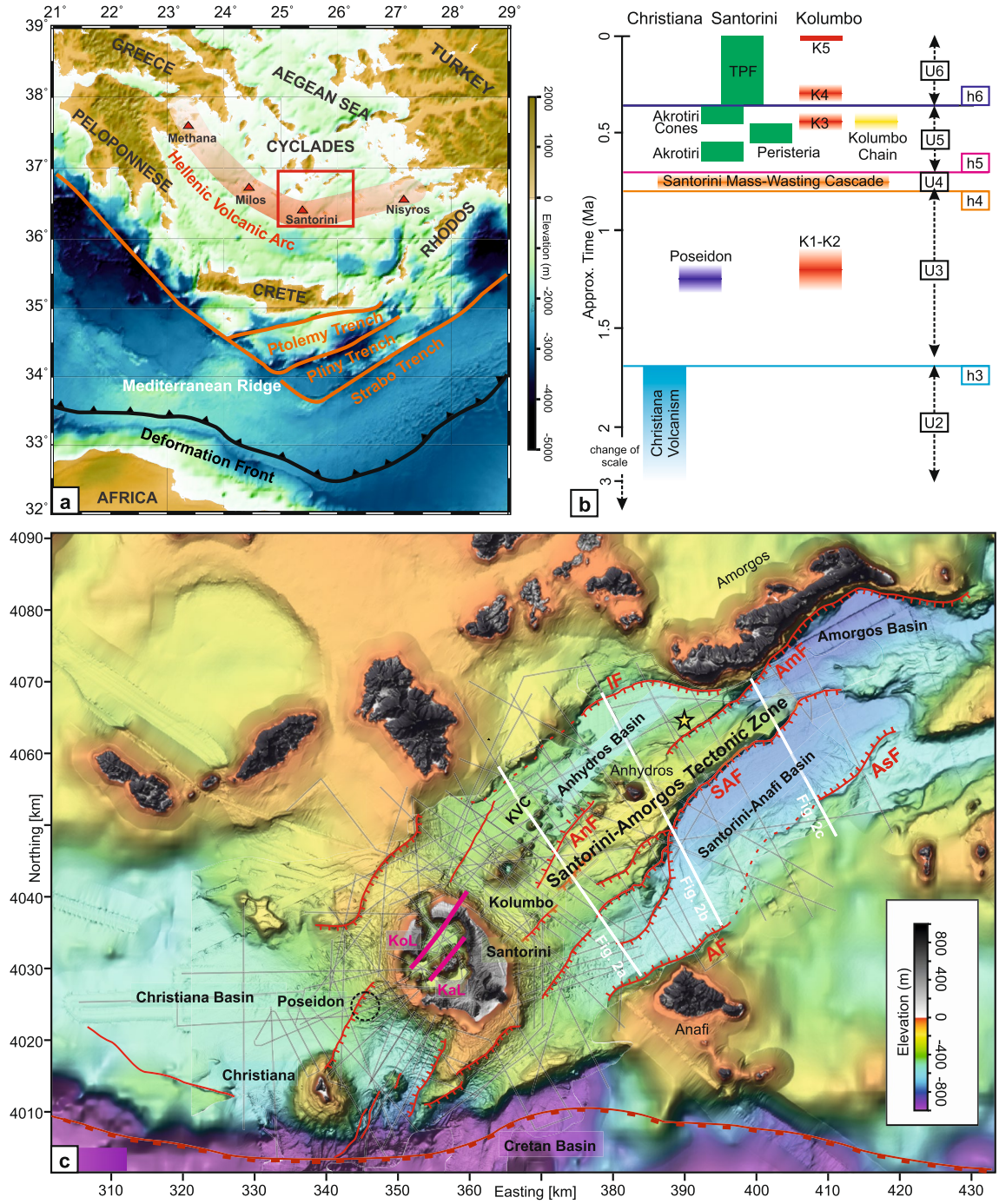

Figure 1. (a) Southern Aegean Sea and major structural features of the Hellenic Arc. Modified from Jolivet et al. (2013), Bocchini et al. (2018), and Preine et al. (2020). Red rectangle shows the study area. (b) Illustration of the spatio-temporal evolution of the CSK volcanic field with estimated ages of major volcanic units, unconformities (h1-h6), and seismostratigraphic units (U2-U6). Modified from Preine, Karstens, Hübscher, Nomikou, et al. (2022). TPF: Thera Pyroclastic Formation; K1-K5: Kolumbo eruptions. (c) Morphological map of the CSK rift zone showing islands, basins, volcanic centers, and major extensional structures after Nomikou, Hübscher, et al. (2016); Nomikou, Hübscher, et al. (2018); Nomikou et al. (2019) and Preine, Karstens, Hübscher, Crutchley, et al. (2022). Bathymetry from Nomikou, Hübscher, et al. (2018); Nomikou et al. (2012, 2013, 2019) and Hooft et al. (2017). Topography from the Hellenic Military Geographic Service. Gray lines show all seismic profiles, white lines indicate the locations of seismic profiles shown in Figure 2. Red lines indicate faults, and purple lines indicate the Kameni and Kolumbo Lines. Yellow star indicates the location of the first Amorgos 1956 earthquake from Okal et al. (2009). Dashed black circle indicate location of buried Poseidon center (Preine, Karstens, Hübscher, Nomikou, et al., 2022). KVC: Kolumbo Volcanic Chain; KoL: Kolumbo Line; KaL: Kameni Line; AF: Anafi-Fault; AmF: Amorgos Fault; AnF: Anhydros Fault; AsF: Astypalaea Fault; IF: Ios Fault; SAF: Santorini-Anafi Fault.

extension in the back-arc and forearc Aegean region leading to the formation of NE-SW directed fault systems (e.g., Bocchini et al., 2018; Gautier et al., 1999; Papazachos, 2019; Van Hinsbergen & Schmid, 2012). Prominent examples of these fault systems are the deep Ptolemy, Pliny, and Strabo Trenches in the forearc region (Figure 1a), or the prominent Santorini-Amorgos Tectonic Zone (SATZ) in the back-arc region (Figure 1c) (Nomikou, Hübscher, et al., 2018).

Located in the center of the Hellenic Arc, the 100 km long and 45 km wide CSK rift zone represents a major structural boundary separating the Hellenic Arc into a volcanically and tectonically active eastern and a quiet western part (Bohnhoff et al., 2006). It is situated at the junction of the Christiana Basin in the west and the SATZ in the east (Figure 1c). The northeastern basins (Anhydros, Santorini-Anafi, and Amorgos) are NE-SW striking grabens and half-grabens with sediment infill up to 1,400 m thick that are bounded by major extensional to transtensional faults with fault throws exceeding 2,000 m (Figure 1c) (Bohnhoff et al., 2006; Hübscher et al., 2015; Nomikou, Hübscher, et al., 2016; Nomikou, Hübscher, et al., 2018; Preine et al., 2020). The Anhydros Basin contains the submarine Kolumbo Volcano and the Kolumbo Volcanic Chain (Figure 1c), whereas the Santorini-Anafi and Amorgos Basins lack volcanoes (Figure 1c). Opening of these basins occurred in multiple episodes of enhanced rift activity, so-called 'tectonic pulses' (Hübscher et al., 2015; Preine, Karstens, Hübscher, Crutchley, et al., 2022). The Anhydros and Anafi Basins each contain six seismostratigraphic units separated by onlap surfaces while the Amorgos Basin only contains the uppermost four units (Hübscher et al., 2015; Nomikou, Hübscher, et al., 2016; Nomikou, Hübscher, et al., 2018; Nomikou et al., 2019).

Southwest of Santorini lies the Christiana Basin, which hosts the Christiana Volcano and several volcanic domes (Figure 1c) (Hooft et al., 2017; Nomikou et al., 2013). This basin is assumed to have formed prior to the basins NE of Santorini under an older E-W striking fault system (Heath et al., 2019; Piper et al., 2007; Preine, Karstens, Hübscher, Nomikou, et al., 2022). However, recent studies have shown that the NE-SW-directed fault trend of the northeastern rift basins continues underneath Santorini, with a prominent fault extending from Santorini towards Christiana (Figure 1c) (Heath et al., 2019; Preine, Karstens, Hübscher, Nomikou, et al., 2022; Preine, Karstens, Hübscher, Crutchley, et al., 2022). Approx. 0.7 Ma ago, the entire rift system was affected by an intensive tectonic pulse, triggering a cascade of sector collapses and secondary mass-wasting events at Christiana and Santorini (Figure 1b) (Preine, Karstens, Hübscher, Crutchley, et al., 2022).

2.2. Volcanic Background

The present-day Hellenic Volcanic Arc initiated 3–4 Ma ago and stretches from the Gulf of Saronikos in the west through Milos, the CSK field, to the Kos-Nisyros-Yali complex in the east (Figure 1a) (e.g., Nomikou et al., 2013; Pe-Piper & Piper, 2007). The CSK field comprises the extinct Christiana Volcano, the Santorini Caldera, the polygenetic submarine Kolumbo Volcano, as well as the Kolumbo Volcanic Chain (Figure 1c) (Nomikou et al., 2019; Preine, Karstens, Hübscher, Nomikou, et al., 2022). Having produced over 100 explosive eruptions in the last 360 kyrs, the CSK field is one of the most hazardous volcanic systems in Europe (Druitt et al., 1999). At least four major caldera-forming eruptions have occurred at Santorini, with the most recent caldera-forming eruption, the 3,600 ka "Minoan" eruption, being considered one of the largest in the Holocene (e.g., Druitt et al., 1999; Johnston et al., 2014; Nomikou, Druitt, et al., 2016).

The CSK field is assumed to have evolved during four main phases of volcanic activity (Figure 1b) (Preine, Karstens, Hübscher, Nomikou, et al., 2022). The first phase initiated in the Pliocene with the formation of the Christiana volcano, which became inactive at ∼1.6 Ma (Figure 1b) (Heath et al., 2019; Piper et al., 2007; Preine, Karstens, Hübscher, Nomikou, et al., 2022). In the second phase, volcanism aligned NE-SW and focused on the early Kolumbo and the Poseidon centers (Figure 1b) (Hübscher et al., 2015; Preine, Karstens, Hübscher, Nomikou, et al., 2022). Both centers produced volcanoclastic deposits that are intercalated within the sedimentary strata of the hosting Christiana and Anhydros Basins. A distinct change in the volcanic behavior occurred at ∼0.7 Ma after the Santorini mass-wasting cascade occurred that transported up to 125 km³ of sediments from Christiana and Santorini into the surrounding basins (Figure 1b) (Preine, Karstens, Hübscher, Crutchley, et al., 2022). Afterward, in the third phase, volcanism occurred throughout the entire CSK field forming a series of volcanic cones, as well as the onshore exposed Akrotiri rhyolitic centers, the Peristeria stratovolcano, and the Akrotiri cinder cones (Figure 1b) (Preine, Karstens, Hübscher, Nomikou, et al., 2022). Another pronounced change in the volcanic system occurred in the fourth phase approx. 360 ka ago, when volcanism focused on the northern part of Santorini and became highly explosive while Kolumbo remained active (Figure 1b). The

products of Santorini during this last and ongoing phase are referred to as the Thera Pyroclastic Formation and are largely exposed on the caldera cliffs (Figure 1b) (Druitt et al., 1999). Offshore, these deposits are recognized as a very thick (~350 m) wedge north of Santorini that thins out towards the Anhydros Basin and the Christiana Basin (Preine, Karstens, Hübscher, Nomikou, et al., 2022). This latest phase correlates to a distinct change in the primitive-melt diversity that occurred between ~360 ka and 224 ka (Flaherty et al., 2022). Volcanism during this latest phase focused on the Kolumbo and Kameni Lines (Figure 1c), which bound a low-velocity anomaly interpreted as a shallow magma body at 3–5 km depth (Heath et al., 2019; Hooft et al., 2019; McVey et al., 2020).

3. Methods

During six cruises between 2006 and 2019, we collected an extensive dataset of over 3,200 km of high-resolution multi- and single-channel seismic data (Figure 1c) (Hübscher et al., 2006; Karstens et al., 2020; Sigurdsson et al., 2006). For all multichannel seismic profiles, we applied multiple removal by means of surface-related multiple elimination and pre-stack time migration. See Supporting Information S1 for more details regarding the acquisition and processing of the seismic data. All processed seismic profiles were combined into an interpretation project using KingdomSuite software. Here, we established the stratigraphic framework (Figure 2) (following the nomenclature in Preine, Karstens, Hübscher, Nomikou, et al., 2022), mapped seismic units, and created isochron maps (vertical thickness in two-way travel time) by interpolating between the seismic profiles (Figure 3). We converted the isochron maps to isochore maps in meters by using constant interval velocities derived from diffraction-based wavefront tomography (see Table S3 in the Supporting Information S1; Preine et al., 2020). These interval velocities do not account for lateral velocity changes and should therefore be considered approximations. In addition, we created reconstructions of the rift basin evolution by flattening key horizons (Figure 4). This simple method levels the seismic profile to an interpreted horizon, which allows the effects of fault displacements to be reversed and, thereby, obtain insights into the deformation of the sediments beneath the examined horizons during the time of its deposition (e.g., Jamaludin et al., 2015; Nuuns, 1991). Horizon flattening is available as a standard interpretation tool in the KingdomSuite software.

4. Results

4.1. Seismostratigraphy of the Rift Basins

Different seismostratigraphic interpretations for basins surrounding the CSK field have been presented in previous studies focusing on different parts of the area, e.g. the Anhydros Basin (Hübscher et al., 2015; Nomikou, Hübscher, et al., 2016) the eastern SATZ (Nomikou, Hübscher, et al., 2018, 2019) or the Christiana Basin (Tsampouraki-Kraounaki & Sakellariou, 2018). In the following, we will use a previously defined seismostratigraphic framework for the entire CSK rift zone (Preine, Karstens, Hübscher, Nomikou, et al., 2022; Preine, Karstens, Hübscher, Crutchley, et al., 2022). This seismostratigraphic framework comprises six units separated by six key horizons h1-h6 (see Table S4 in the Supporting Information S1 for a detailed comparison of the different seismostratigraphic frameworks). These horizons are high-amplitude reflections, which lie conformable outside the rift basins but represent major unconformities inside the rift basins. Approximate ages of the seismo-stratigraphic units have been estimated by Preine, Karstens, Hübscher, Nomikou, et al. (2022) and are based on correlations with onshore volcanic products and the extrapolation of sedimentation rates (for an overview, see Figure 1b). However, due to the lack of direct samples, these ages od deeper units are associated with considerable uncertainties.

The lowermost unit (Unit 1) is characterized by weakly reflective strata with sub-parallel reflections that have been interpreted to be of Pliocene age (Figure 1b) (Preine, Karstens, Hübscher, Nomikou, et al., 2022). Unit 1 is covered by Unit 2, which comprises a series of well-stratified reflections with medium to high amplitudes and is considered to be of Late Pliocene/Early Pleistocene age (Figure 1b). Unit 3 and Unit 5 consist of a sequence of well-stratified reflections with medium amplitudes, which contrast with the weakly reflective nature of Unit 4, which has been interpreted as the deposits of the Santorini Mass-Wasting Cascade (Preine, Karstens, Hübscher, Crutchley, et al., 2022). In the vicinity of Santorini, the uppermost Unit 6 comprises high-amplitude irregular reflections that comprise volcano-sedimentary deposits from the Thera Pyroclastic Formation during the last 0.36 Ma (Figure 1b) (Preine, Karstens, Hübscher, Nomikou, et al., 2022).

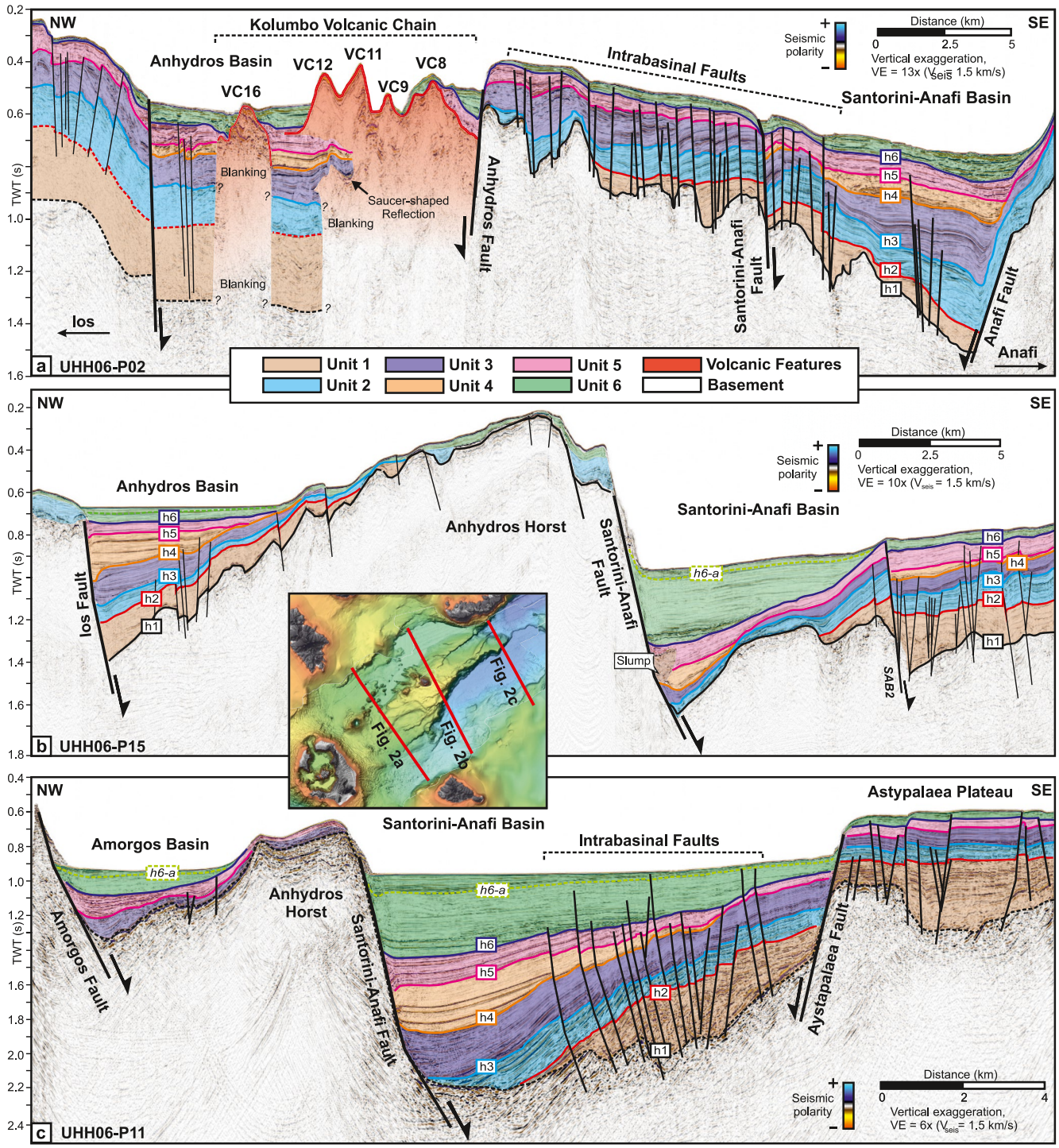

Figure 2. Seismic profiles crossing the Santorini-Amorgos Tectonic Zone. For locations, see inset map. Semi-transparent colors indicate different seismic (U1-U6) and volcanic units as indicated in the legend on top. VE – vertical exaggeration. (a) Profile UHH06-P02 crossing the western Anhydros Basin, the Kolumbo Volcanic Chain, and the western Santorini-Anafi Basin. SAB2: Major Fault within the Santorini-Anafi Basin. (b) Profile UHH06-P15 profile crossing the eastern Anhydros Basin, the Anhydros Horst, and the central Santorini-Anafi Basin. (c) Profile UHH06-P11 profile crossing the western Amorgos Basin, the Anhydros Horst, and the eastern Santorini-Anafi Basin.

Figure 2 shows three seismic profiles crossing the SATZ approx. perpendicular to the NE-SW-directed main fault trend (Nomikou, Hübscher, et al., 2018). Semi-transparent colors indicate seismostratigraphic Units 1–6 (for an un-interpreted version of the profiles, see Figure S2 in the Supporting Information S1). Profile A (UHH06-P02)

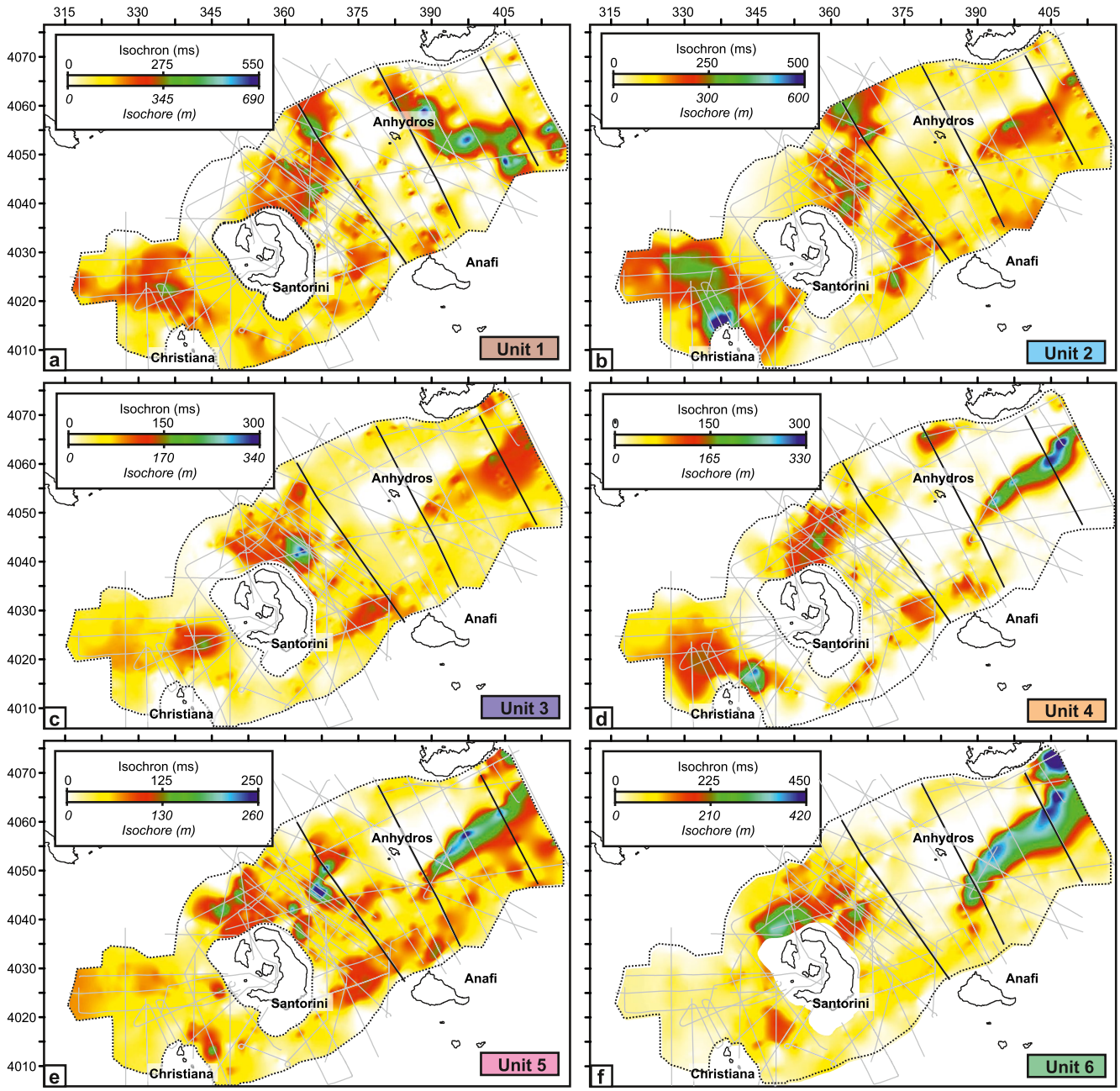

Figure 3. Isochrone and approximated isochore maps of Units 1–6 as interpolated from seismic lines highlighted in gray. Black lines indicate the location of seismic lines shown in Figure 2. Present-day coastlines for spatial reference.

crosses the Kolumbo Volcanic Chain in the Anhydros Basin as well as the Santorini-Anafi Basin and terminates in front of the island of Anafi (Figure 2a). The internal architecture of these two basins differs significantly (Figure 2a). While the Santorini-Anafi Basin represents a SE-ward tilted half-graben bounded to the NW by the Santorini-Anafi Fault with the sedimentary infill thickening towards the Anafi Fault, the Anhydros Basin represents a graben bounded by steeply dipping faults and is strongly overprinted by the volcanism of the Kolumbo Chain masking significant parts of the deeper strata (Figure 2a). The basement reflection h1 is barely visible here, which is in contrast with the Santorini-Anafi Basin, where h1 is a well-defined high-amplitude reflection and the entire sedimentary strata is well-imaged (Figure 2a). While the Anafi Fault has a throw exceeding 1,000 m here, the Santorini-Anafi Fault is only a small throw of ~100 m (Figure 2a).

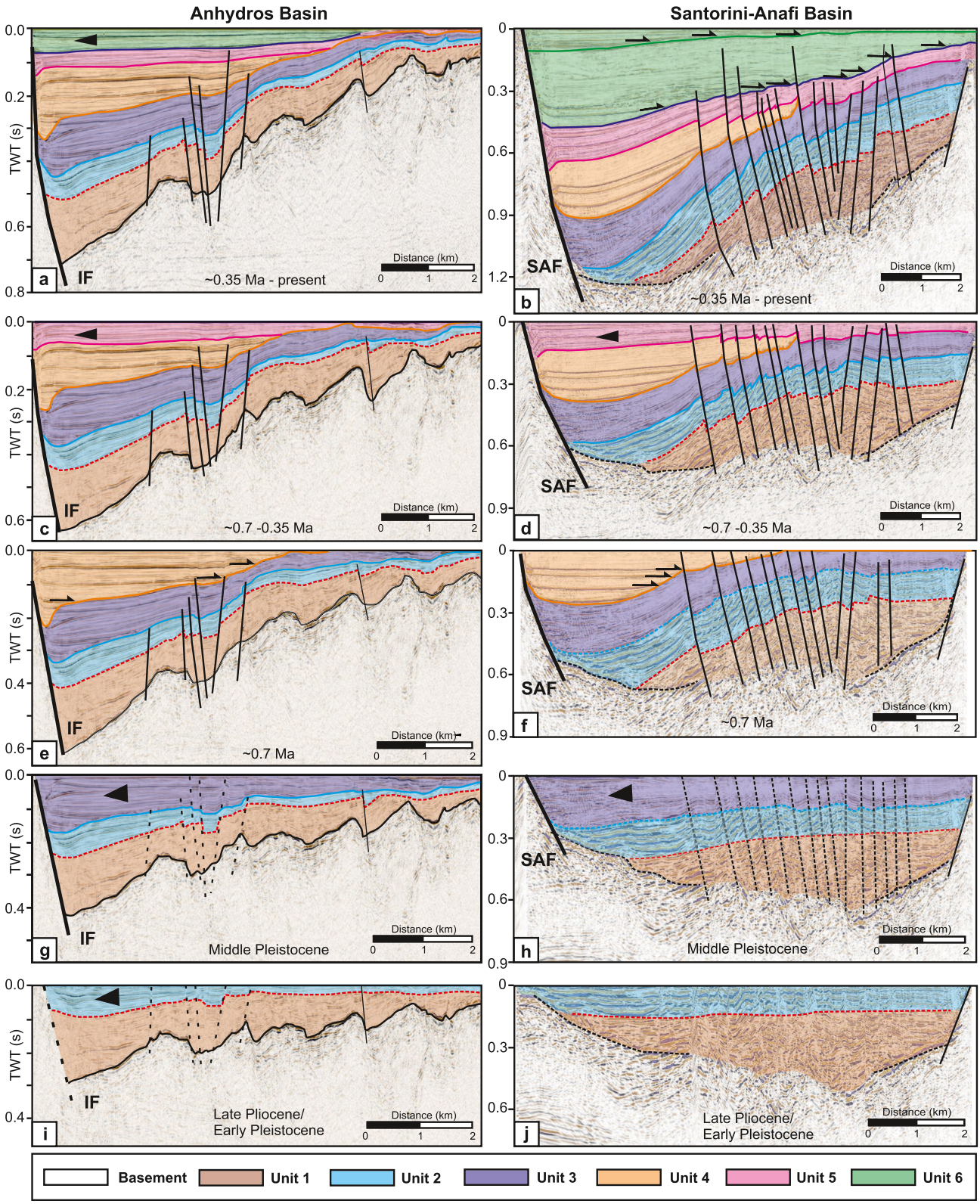

Figure 4. Reconstruction of the Anhydros Basin (a, c, e, g, i) and the Santorini-Anafi Basin (b, d, f, h, j) by successively flattening the top of each Unit in Figures 2b and 2c. Arrows indicate onlap termination and triangles indicate divergence. Approximate ages of the seismostratigraphic units are from Preine, Karstens, Hübscher, Nomikou, et al. (2022). SAF: Santorini-Anafi Fault; IF: Ios Fault.

In general, the sedimentary infill of the Anhydros Basin shows a uniform thickness (Figure 2a). While Units 1 and 2 are thick here (>200 ms TWT/ ~250 m), Units 3–6 are rather thin (<100 ms TWT/ ~110 m) (Figure 2a). There are multiple volcanic cones belonging to the Kolumbo Chain, which are labeled VC# according to Nomikou et al. (2012) (Figure 2a). Edifice VC16 has distinct high-amplitude reflections at the top reaching the seafloor, while seismic blanking occurs underneath (Figure 2a). Further towards the SE, we identify four volcanic cones VC12, VC11, VC 9, and VC8, which pinch out within Unit 5. While VC8 is buried by Units 6 and 5, volcanic cones VC12, VC11, and VC9 breach the seafloor and are overlain by only a thin sediment cover (Figure 2a). Towards the Anhydros Fault, the underlying strata is strongly disturbed and only some irregular high-amplitude reflections are visible. Beneath volcanic cone VC12 is a buried volcanic edifice that pinches out within Unit 3 and is marked by a saucer-shaped high-amplitude reflection (Figure 2a).

Southeast of the Anhydros Fault is a strongly faulted zone, with many steeply-dipping (~60°) faults that have throws of 10–30 m (Figure 2a). Towards the Anafi Fault, Unit 3 thickens significantly, while having a rather constant thickness elsewhere (Figure 2a). Unit 4 represents a thick deposit in the Santorini-Anafi Basin (~90 ms TWT/ ~200 m), but it thins out towards the NW (Figure 2a). While Unit 5 has a rather constant thickness, Unit 6 is thickening towards the Anafi Fault (Figure 2a). Here, we observe high-amplitude irregular reflections representing the volcano-sedimentary deposits from the Thera Pyroclastic Formation (Figure 2a) (Preine, Karstens, Hübscher, Nomikou, et al., 2022; Preine, Karstens, Hübscher, Crutchley, et al., 2022).

Profile B (UHH06-P15) crosses the Anhydros and Santorini-Anafi Basins in the central part of the SATZ close to the Anhydros Islet, which is part of the Anhydros Horst (Figure 2b). Here, the Anhydros Basin lacks volcanic structures and represents a typical half-graben bounded by the Ios Fault, which has a throw of ~700 m (Figure 2b) (Hübscher et al., 2015; Nomikou, Hübscher, et al., 2018). We identify all six Units in this basin, with Units 3 and 4 showing a pronounced thickness increase towards the Ios Fault, while Units 5 and 6 have a rather constant thickness (Figure 2b). Reflections h6 and h5 lie flat and onlap reflection h4, which has a distinctly different dip that lies sub-parallel to that of the underlying reflectors h3, h2, and h1 (Figure 2b). The Anhydros horst is overlain by a sequence of thin sediments with some faults piercing the seafloor (Figure 2b).

SE of this horst, the seafloor of the Santorini-Anafi Basin is deeper than that of the Anhydros Basin and the internal architecture of both basins contrasts strongly (Figure 2b). The Santorini-Anafi Fault is associated with a major throw, which offsets the basement up to 1.2 km here (Figure 2b). In the central Santorini-Anafi Basin, Unit 6 is very thick (~350 ms TWT/ ~320 m) at the foot of the Santorini-Anafi Fault, while thinning dramatically towards the SE where its thickness is only (~50 ms TWT/ ~45 m) (Figure 2b). It comprises a set of low-amplitude reflections that onlap horizon h6 (Figure 2b). At the top of Unit 6, we identify a distinct high-amplitude reflection (h6-a), and at the base, we identify several irregular high-amplitude reflections (Figure 2b). The internal reflections of Unit 6 are mostly sub-parallel to the seafloor while the deeper reflections (h6-h2) show a pronounced dip towards the Santorini-Anafi Fault (Figure 2b). Unit 5 thickens towards the foot of the Santorini-Anafi Fault, where we identify a confined area with irregular reflections interpreted as a slump deposit originated from the Santorini-Anafi Fault (Figure 2b) (Nomikou, Hübscher, et al., 2018; Preine, Karstens, Hübscher, Crutchley, et al., 2022). Unit 4 is only present at the foot of the Santorini-Anafi Fault and pinches out towards the SE onlapping the underlying unconformity h4 (Figure 2b). Towards the SE on the shoulder of the basin, there is a distinct SE-wards dipping fault (labeled 'SAB2') that marks a distinct change in the internal architecture of the basin infill (Figure 2b). Here, the deeper Units 1–3 are thicker and strongly faulted while thinning out towards the NW (Figure 2b).

Profile C (UHH06-P11) crosses the western tip of the Amorgos Basin and the northeastern Santorini-Anafi Basin, which represents a graben defined by the Santorini-Anafi Fault (throw of >1.4 km) and the Astypalaea Fault (throw of >400 m) (Figure 2c) (Nomikou, Hübscher, et al., 2018). The Anhydros Horst, which separates both basins, has a much smaller lateral extent here compared to Profile B (Figure 2b). We identify all six seismostratigraphic units within the Santorini-Anafi Basin while the Amorgos Basin lacks Units 4, 2, and 1 (Figure 2c). Similar to Profile B, Unit 6 is very thick (~400 ms TWT/ ~370 m) in the central Santorini-Anafi Basin, while being much thinner on the Astypalaea Plateau (~60 ms TWT/ ~55 m) (Figure 2c). The internal reflections of this uppermost Unit have low amplitudes, show complex sub-parallel/hummocky internal reflections, and onlap the underlying horizon h6, which represents a major unconformity (Figure 2c). Also here, we identify the high-amplitude reflection h6-a at the top of Unit 6, which defines the base of subunit U6-a that that thickens towards the Santorini-Anafi fault. Both, the Santorini-Anafi Basin and the Astypalaea Plateau, are strongly faulted, but offsets are markedly smaller in Unit 1 with some internal faults fading out at unconformity h6 (Figure 2c). The underlying Units 5-3

are strongly thickening towards the Santorini-Anafi Fault, with Unit 4 pinching out towards the Astypalaea Fault (Figure 2c). In contrast to that, Units 1 and 2 have a uniform thickness in the Santorini-Anafi Basin. The Amorgos Basin also contains a thick sequence of Unit 6 (~130 ms TWT/ ~120 m), while the underlying Units 5 and 3 are diverging towards the Amorgos Fault (Figure 2c).

4.2. Mapping of the Seismostratigraphic Units

Combining all seismic profiles throughout the study area (Figure 1c), we created isochrone maps of all seismostratigraphic units by interpolating between seismic profiles (Figure 3). These isochrones maps reveal a succession of depocenters and deposit-free areas that have been active during different times of the evolution of the rift system. The isochrone maps can be converted to isochore thickness maps by applying interval velocities for each Unit (Preine et al., 2020; see Table S3 in the Supporting Information S1). Unit 1 has been deposited in a complex puzzle of depocenters with a main depocenter in the Christiana Basin (Figure 3a). In addition, we identify a large depocenter that extends from the eastern flank of present-day Santorini towards the NNE, which has been crossed by Profile A (Figure 2a). East of the Anhydros islet, we identify a narrow depocenter cross-cutting the present-day Anhydros and Santorini-Anafi Basins (Figure 3a).

Mapping of Unit 2 reveals a main depocenter in the Christiana Basin, as well as a depocenter extending from the NE flank of Santorini towards the island of Ios (Figure 3b). The depocenter in the Christiana Basin is strongly thickening towards the Christiana edifice (Figure 3b), which is mainly due to basin-wards dipping reflections from the Christiana edifice as shown in Preine, Karstens, Hübscher, Nomikou, et al. (2022). There are two additional depocenters at the western and eastern Santorini-Anafi Basin, which are aligned approx. in NE-SW direction. For Unit 3, we identify two distinct, circular depocenters west and east of Santorini at the locations of the Poseidon and early Kolumbo volcanic centers (Figure 3c) (Preine, Karstens, Hübscher, Nomikou, et al., 2022). In addition, we identify a depocenter northwest of Anafi (Figures 2a and 3c) and a depocenter in front of the eastern Santorini-Anafi Fault (Figures 2c and 3c). Both depocenters are aligned NE-SW, parallel to the present-day fault trend (Nomikou, Hübscher, et al., 2018).

The isochore map of Unit 4 has already been presented in Preine, Karstens, Hübscher, Crutchley, et al. (2022) and comprises eight separated depocenters (Figure 3d). This is well visible in Figure 2, where Unit 4 occurs only in the basin centers next to major faults. For Unit 5, we identify a major depocenter at the eastern Santorini-Anafi Basin, where a distinct thickening towards the Santorini-Anafi Fault is observed (Figures 2c and 3e). There are several depocenters along the Kolumbo volcanic chain (Figure 3e), which evolved contemporarily to the deposition of Unit 5 (Preine, Karstens, Hübscher, Nomikou, et al., 2022). The same applies to a distinct depocenter west of Santorini, representing the deposits of the Aspronisi cones (Figure 3e) (Preine, Karstens, Hübscher, Nomikou, et al., 2022). Additional depocenters are located north of Santorini, between Santorini and Anafi, and east of Christiana (Figure 3e).

The isochore map of Unit 6 reveals a broad depocenter in the Santorini-Anafi Basin (Figure 3f) that has been crossed by Profiles B and C (Figures 2b and 2c). This depocenter covers the eastern Santorini-Anafi Basin and extends towards the Amorgos Basin in the NE, where it reaches its maximum thickness (>400 m) (Figure 3f). In addition, there is a distinct depocenter north of Santorini that is interpreted to be the deposits of the Thera Pyroclastic Formation.

5. Discussion

5.1. Basin Opening

As described previously, the six key horizons h1-h6 represent major unconformities in the rift basins marking distinct phases of episodic basin-opening. In order to highlight the dynamics of these tectonic episodes, Figure 4 illustrates the eastern Anhydros Basin from Profile B (Figure 2b) and the eastern Santorini-Anafi Basin from Profile C (Figure 2c) after successive flattening of key horizons h1-h5 (Figure 3). This method allows to visualize the approximate geological situation during deposition of each flattened horizon and thereby to reconstruct the general basin evolution (Jamaludin et al., 2015). In contrast to methods like structural restoration, horizon flattening does not take into account slip across faults that intersect horizons or compaction during deposition

(Nuuns, 1991). However, structural restoration requires detailed information about the physical properties of each seismostratigraphic unit, which are typically only available from drilling campaigns.

In general, we distinguish two types of basin-opening in the context of the Santorini-Amorgos Tectonic Zone: continuous hanging-wall rotation vs. tectonic pulses. Continuous hanging-wall rotation implies that the fault-induced subsidence occurs on time scales that allow syn-tectonic deposition, which would manifest as divergent internal reflections. In contrast to that, tectonic pulses are defined by distinct episodes of hanging-wall rotation of the marginal faults, which occur so fast that no seismically resolvable syn- tectonic deposition is detectable. Instead, the subsequently deposited strata laps onto the horizon marking the pulse event. Hübscher et al. (2015) have shown the occurrence of multiple distinct tectonic pulses in the Anhydros Basin, while Preine, Karstens, Hübscher, Crutchley, et al. (2022) showed that a rift-wide tectonic pulse preceded the emplacement of Unit 4, the Santorini Mass-Transport Deposit.

The tectonics of the Anhydros Basin shows low activity during the deposition of the two uppermost units, 6 and 5, which are well-stratified and only have a minor thickness increase towards the Ios Fault (Figures 4a and 4c). In contrast to that, there was a distinct tectonic pulse before the deposition of Unit 4. As highlighted in Figure 4d, the internal reflections of Unit 4 are parallel to the flattened top of the Unit, while the underlying unconformity h4 reveals a distinct dip, on which the internal reflections onlap. The divergence of internal reflections towards the Ios Fault during deposition of Unit 3 implies a continuous basin opening and tilting (Figure 4g). This also applies to Unit 2, which is generally thin inside the Anhydros Basin but also shows divergence towards the Ios Fault (Figure 4e). For Unit 1, there also seems to be divergence towards the Ios Fault, although imaging becomes more difficult here obscuring the internal architecture of this unit (Figure 4i).

In contrast to the Anhydros Basin, the Santorini-Anafi Basin was highly active during deposition of Units 5 and 6. As shown in Figures 2b, 2c, and 4b, Unit 6 is very thick in the Santorini-Anafi Basin while being very thin on the shoulders of the basin. At the top of Unit 6, we identify indications for a recent tectonic event that is marked by the uppermost subunit U6-a, which comprises a set of high-amplitude reflections that contrast with the weakly reflective nature of the rest of Unit 6 (Figure 4b). Internal reflections onlap horizon u6-a indicating that this uppermost subunit might represent a very recent tectonic pulse (Figure 4b). We identify this uppermost subunit U6-a only in the eastern Santorini-Anafi Basin in Profiles B and C and in the Amorgos Basin in Profile C (Figures 2a and 2c). This indicates that tectonic deformation in the most recent phase focused on the eastern Santorini-Amorgos Tectonic Zone. Recent tectonic deformation in this area has been underlined by the 1956 Amorgos earthquake whose epicenter has been associated with the Amorgos Fault (Figure 1c) (Nomikou, Hübscher, et al., 2018). However, our seismostratigraphic framework does not allow us to place this unconformity into the age model from Preine, Karstens, Hübscher, Nomikou, et al. (2022) to tie down the onset of this most recent tectonic pulse.

In addition to that, we identify indications for a major tectonic pulse at the transition of Units 5 and 6 due to the distinct onlap termination of the internal reflections of Unit 6 towards the underlying unconformity h6, which has a markedly different dip (Figure 4b). The irregular high-amplitude reflections at the base of Unit 6 indicate that this tectonic pulse was accompanied by a high-energetic erosional event (Figure 4b) (Preine et al., 2020). In addition, many internal faults have much lower displacements above h6 (<5 ms TWT/ ~5 m) than below it (>20 ms TWT/ ~22 m) indicating that either internal faulting has ceased mostly after the deposition of h6, or that subsequent deposition occurred very rapidly in relation to the rate of faulting. Assuming an age of ~0.36 Ma for unconformity h6 (Preine, Karstens, Hübscher, Nomikou, et al., 2022) implies a rapid deposition of Unit 6 with sedimentation rates in the order of ~1 m/kyr, which is approx. 5 to 10 times the measured sedimentation rates of the Quaternary across the CSK volcanic rift zone (Anastasakis & Piper, 2005; Kutterolf et al., 2021; Piper & Perissoratis, 2003). Such enhanced sedimentation rates have also been proposed by previous studies (Perissoratis, 1995; Piper & Perissoratis, 2003) for the Santorini-Anafi region and could be explained by assuming that the Santorini-Anafi Basin has been a major depocenter for volcanoclastic material from Santorini, which has been highly active during the last 0.36 Ma producing the vast Thera Pyroclastic Formation (Druitt et al., 1999). Therefore, the complex internal reflections of Unit 6 in the Santorini-Anafi Basin (Figures 2c and 4b) could represent volcanoclastic infill deposits e.g. from pyroclastic flows or remobilized volcanoclastic material.

During deposition of Unit 5, the Santorini-Anafi Fault remained active as indicated by a distinct thickening of the strata towards the NW (Figure 4d). As shown in Figures 2b, a major slump deposit is intercalated within Unit 5, which seems to be associated with the activity of the Santorini-Anafi Fault highlighting pronounced tectonic

activity during that time. Similar to the Anhydros Basin, we observe that the internal reflections of Unit 4 appear perfectly flat and clearly onlap the underlying unconformity h4 after flattening horizon h5 (Figure 4f). This underlines the concept of a major tectonic pulse happening before the deposition of the mass-transport deposits of Unit 4 (Figure 4f). In contrast, Unit 3 below shows significant divergence towards the Santorini-Anafi Fault indicating that this fault was continuously active during deposition of Unit 3 (Figure 4h). Notably, the offsets between internal faults are mostly leveled after flattening horizon h3, which suggests that these faults formed after the deposition of Unit 3 (Figure 4h). Unit 2 lies flat in the Santorini-Anafi Basin, while Unit 1 seems to be thickening towards the SW, although its internal architecture is difficult to properly image (Figure 4j).

5.2. Volcano-Tectonic Evolution of the CSK Rift Zone

Figure 5 shows a sketch of the volcano-tectonic evolution of the CSK rift zone as interpreted from our seismostratigraphic framework. Fault activity is inferred from observed thickness differences at individual faults. Ages of different seismostratigraphic Units and the spatio-temporal evolution of the CSK volcanic centers are based on Preine, Karstens, Hübscher, Nomikou, et al. (2022), whose four major volcanic phases occurred during the deposition of Units 2, 3, 5, and 6 (see Figure 1b for an overview). The lowermost Unit 1 represents the deposits of Early Pliocene marine ingression across the southern Aegean and is considered pre-volcanic (Preine, Karstens, Hübscher, Nomikou, et al., 2022) (Figure 5a). Our mapping shows that this unit has been deposited in a complex environment with two roughly WNW-ESE striking depocenters in the Christiana Basin and east of the Anhydros Islet (Figure 5a). This fault trend fits the general E-W trend that has been proposed for the Pliocene basins of the southern Aegean (Figure 5a) (e.g., Anastasakis & Piper, 2005; Piper et al., 2007). Both depocenters are separated by a broader NNE-SSW trending zone, which underlies the present-day centers of Kolumbo and the Kolumbo volcanic chain (termed 'proto-Anhydros Basin', in accordance with Heath et al., 2019). The presence of a deep proto-Anhydros Basin is supported by deep P-wave seismic tomography indicating that a NE-SW striking basin existed underneath present-day Santorini, Kolumbo, and Christiana (Heath et al., 2019).

Assuming that the dominant extension during that time was oriented NNE-SSW (Figure 5a), implies that this basin might have acted as a transfer zone between WNW-ESE trending fault systems. Similar north-south trending transfer zones have been observed at other centers of the Hellenic Volcanic Arc, e.g. at Milos (Anastasakis & Piper, 2005) or Nisyros (Papanikolaou & Nomikou, 2001), and have also been suggested for Santorini (Heath et al., 2019; Piper et al., 2007). This depocenter might have been a dextral pull-apart basin that accommodated N-S directed strain between the basins west and east of present-day Santorini (Figure 5a). However, the volcanic overprint in the Anhydros Basin prohibits a detailed analysis of fault geometries (e.g., Figure 2a).

During the deposition of Unit 2 in the Late Pliocene/Early Pleistocene, volcanism initiated with the emergence of the Christiana Volcano (Figure 5b) (Preine, Karstens, Hübscher, Nomikou, et al., 2022). During this time, the Christiana Basin continued to be a major WNW-ESE-oriented depocenter, and the distinct thickening towards Christiana observed in Figure 3b represents the volcanoclastic deposits exported from Christiana (Figure 5b). Our mapping of Unit 2 indicates that the Christiana Basin terminates against an NNE-SSW trending boundary (Figures 3a and 5e), which fits the trend of the proto Anhydros Basin mapped northeast of Santorini. This can be seen as an indication of a continuation of the proto-Anhydros Basin underneath Santorini as indicated by dotted, orange lines in Figure 5b delineated from p-wave tomography (Heath et al., 2019). This fits the trend of our reflection seismic mapping of a proto-Anhydros Basin well. Furthermore, Heath et al. (2019) proposed that the volcanism at Christiana might have been localized by the intersection of the proto Anhydros Basin and the Christiana Basin, which is in agreement with our analysis.

East of Santorini, we identify two NE-SW directed depocenters, which we interpret as the early representations of the present-day Santorini-Anafi Basin ('proto Santorini-Anafi Basin', Figure 5b). These depocenters lie parallel to the present-day faults of the SATZ, which suggests that Unit 2 marks a transitional phase where the stress regime rotated counterclockwise from NNE-SSW to NNE-SSE (Figure 5b). Given that the ESE-WNW oriented Pliocene basin mapped with Unit 1 east of Anhydros (Figure 5a) is no longer identifiable in Unit 2, the tectonic nature of the proto Anhydros Basin during that time remains elusive.

During deposition of Unit 3, the second volcanic phase emerged with the evolution of the early Poseidon and Kolumbo volcanic centers (Figure 5c) (Preine, Karstens, Hübscher, Nomikou, et al., 2022). Our data clearly show that during that time, NE-SW-oriented depocenters became dominant throughout the entire SATZ including

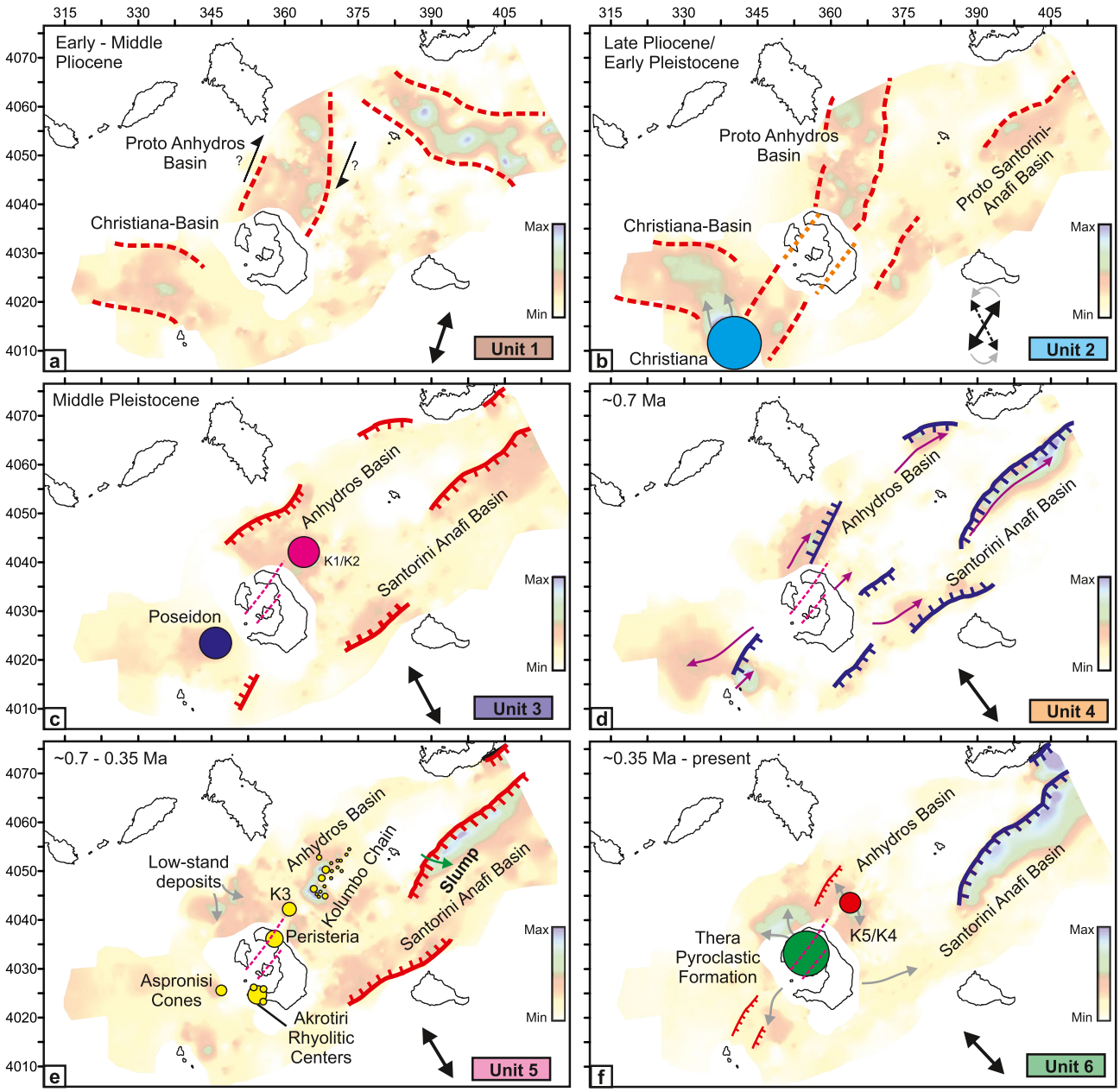

Figure 5. Schematic reconstruction of the volcano-tectonic evolution of the CSK rift zone. Isochore maps from Figure 3 are plotted in the background. Red toothed lines indicate faults active during deposition of each phase. Blue lines indicate faults that have been affected by tectonic pulses. Dashed lines indicate the outline of depocenters with higher uncertainty. Dashed orange lines indicate the outline of the proto-Anhydros Basin underneath Santorini as defined in Heath et al. (2019). Activity of volcanic centers modified from Preine, Karstens, Hübscher, Nomikou, et al. (2022). Black arrows indicate approx. direction of extension as inferred from the interpreted faults. Black arrows in F indicate the potential strike-slip movement of the Proto Anhydros Basin. Thin gray arrows indicate the direction of transport of volcanoclastic material and purple arrows indicate the direction of mass-wasting events (Preine, Karstens, Hübscher, Crutchley, et al., 2022).

activity of the eastern Santorini-Anafi Fault, the eastern Anhydros Fault, and the Anafi Fault (Figure 4d). This activity seems to have been continuous as indicated by the divergence observed within Unit 3 in the Anafi, Santorini-Anafi and Anhydros Basins (Figures 2a–2c, 4g, and 4h). The Poseidon and Kolumbo centers aligned parallel to this new fault trend implying a significant influence of this newly emerging NE-SW-oriented tectonic trend on the magma emplacement. This early NE-SW alignment of volcanic centers could represent an early expression of the present-day Kameni and Kolumbo Lines (dashed line in Figure 5c), which consequently are deep-rooted, old volcano-tectonic lineaments (Preine, Karstens, Hübscher, Nomikou, et al., 2022).

Initiated by an extensive rift pulse that affected the entire rift system, vast amounts of volcano-sedimentary material from Unit 4 were deposited in the basins surrounding Santorini (Figure 4c; Preine, Karstens, Hübscher, Crutchley, et al., 2022). During the deposition of Unit 5 (~0.7–0.36 Ma), volcanism occurred along the entire Christiana-Santorini-Kolumbo field and included the emergence of the Aspronisi cones, the Kolumbo volcanic chain, Kolumbo's Unit K3 as well as the evolution of the Akrotiri rhyolitic centers, the Peristeria stratovolcano, and the Akrotiri cinder cones onshore Santorini (Figure 5e) (Druitt et al., 1999; Preine, Karstens, Hübscher, Nomikou, et al., 2022). We argue the preceding rift pulse and subsequent mass-wasting cascade had a major impact on the volcanic system due to crustal fracturing in combination with unloading, leading to wide-spread magmatic ascent. The formation of approximately linearly arranged volcanic cones could be related to intra-basinal fault systems such as those observed in the Santorini-Anafi Basin (Figure 2c), which have formed mainly during deposition of Units 3 to 5.

We observe that during deposition of Unit 5, the eastern Santorini-Anafi and Amorgos Faults were continuously active as highlighted by the syn-tectonic growth strata recorded in the sedimentary basin infills (Figures 4c, 4d, and 5e). This continuous activity led to a major slumping event south of the Anhydros Islet as imaged in Profile B (Figures 2b and 5e). In addition to that, we identify a depocenter north of Santorini that is not related to any tectonic or volcanic activity but represents a wedge of low-stand deposits likely related to Pleistocene sea-level lowstands (e.g., Marine Isotope Stages 12 and/or 16; see Figure S5 in the Supporting Information S1 for an example) (Lisiecki & Raymo, 2005) (Figure 5e).

After the deposition of Unit 5, another distinct change in the volcano-tectonic system occurred (Figure 4a). At the transition from Unit 5 to 6, volcanism became highly explosive producing the vast Thera Pyroclastic Formation (Druitt et al., 1999; Preine, Karstens, Hübscher, Nomikou, et al., 2022). During that time also Kolumbo remained active producing two major eruptions (K4/K5). Our seismostratigraphic framework shows that the transition from Unit 5 to 6 is marked by another major tectonic pulse that affected the eastern Santorini-Anafi Basin as indicated by the angular unconformity h6 (Figures 2b, 2c and 4b). The here proposed h6-rift pulse is in line with a recent study by Flaherty et al. (2022), who showed that a change in melt diversity of the eruptive products of Santorini occurred between ~360 and 225 ka. This indicates that this tectonic event influenced the deep volcanic plumbing system underneath Santorini e.g. by affecting stresses in the deeper crust and, thus, changing fluxes and proportions of primitive melts from deep supply regions (Flaherty et al., 2022).

In addition, during deposition of Unit 6, the complex Kolumbo and Christiana faults also remained active in the vicinity of Santorini (Figure 5f). However, both show only minor throws (<100 m) that decrease from the base of Unit 6 towards the top (Preine, Karstens, Hübscher, Crutchley, et al., 2022). Furthermore, the tilted uppermost subunit U6-a observed in the eastern basins (Figure 2c) points to yet another recent rift pulse within the eastern Santorini-Anafi Basin. While our seismostratigraphic framework does not allow dating this unconformity, it is noteworthy that another distinct change in melt chemistry of Santorini volcanism occurred 22 ka ago during the caldera-forming Cape Riva eruption (Flaherty et al., 2022). This could correspond to the observed recent tectonic pulse in the eastern SATZ, in which case the age of subunit U6-a would fit the estimated age of Unit A1 from Perissoratis (1995), who correlated related their uppermost seismostratigraphic Unit A1 to the Last Glacial Maximum indicating an approx. age of 20.000 years. However, such temporal correlations remain speculative and the change in melt chemistry after the Cape Riva eruption could also be explained by temporal variations in the supply of slab-derived melts and fluids as well as by caldera collapse (Flaherty et al., 2022).

5.3. Volcano-Tectonic Feedback Mechanisms

Having established the temporal correlation of changes in the tectonic system and volcanic behavior, the question remains, whether the tectonic changes triggered the modifications in the volcanic system or vice versa. To answer this with certainty, exact age relations between rifting events and volcanic eruptions are required, which is beyond the temporal resolution of our seismostratigraphic age models. However, there are several reasons to argue that changes in the tectonic system have preceded changes in the volcanic system and, thus, played an important role in the evolution of the CSK volcanic field.

1. The spatial correspondence of the Pliocene proto Anhydros Basin and the major centers of the CSK volcanic field suggests that this early basin represented an initial zone of crustal weakness that facilitated magma ascend. As discussed above, this initial basin seems to have acted as a dextral transfer zone between the

WNW-ESE trending depocenters. The spatial correlation between transfer zones and magmatism has been highlighted in previous studies at other volcanoes (e.g., Corti et al., 2003; Faulds & Varga, 1998). In the case of the CSK volcanic field, it is noteworthy that the proto Anhydros Basin existed prior to the emplacement of volcanic edifices, which is in contrast to the concept that magmatism causes the formation of transfer zones at the CSK rift as observed in other regions (Faulds & Varga, 1998).

2. Chrono-stratigraphic relations indicate that the evolution of the Poseidon and early Kolumbo centers occurred approx. in the middle of the deposition of Unit 3 (Preine, Karstens, Hübscher, Nomikou, et al., 2022), which has been deposited under the influence of the newly emerging NE-SW striking fault system (Figure 5c). According to our study the initiation of these faults preceded the emplacement of Poseidon and early Kolumbo volcanism and continued afterward. This suggests that the NE-SW-directed faults guided magma ascent leading to the evolution of the Poseidon and early Kolumbo centers.
3. A major tectonic reorganization occurred at ∼0.7 Ma and preceded the evolution of the widespread emergence of volcanic edifices during deposition of Unit 5. As mentioned above, the sudden fracturing of the Aegean crust during this rift pulse might have generated pathways for the emplacement of volcanic edifices, which follow the NE-SW-directed tectonic trend (Preine, Karstens, Hübscher, Nomikou, et al., 2022).
4. Our seismostratigraphic framework indicates that the rift pulse at ∼0.36 Ma preceded the deposition of large amounts of volcanoclastic material from Santorini and Kolumbo, indicating that the tectonic change again influenced the volcanic behavior of the CSK rift zone. In this case, this tectonic pulse has been accompanied by a distinct change in melt diversity of the eruptive products of Santorini that might be related to changes in the stresses in the deeper crust (Flaherty et al., 2022).

On the other hand, it is important to note that the non-volcanic basins of the CSK rift zone are characterized by well-defined half-graben and pronounced marginal faults (e.g., at the Santorini-Anafi Basin, the eastern Anhydros Basin, and the Amorgos Basin) with throws of more than 2,000 m (Figures 1c and 3) (Nomikou, Hübscher, et al., 2018), while the basins hosting the CSK volcanoes (the western Anhydros Basin and the Christiana Basin) lack such distinct tectonic features (Figures 1c and 2a). Instead, they are influenced by more complex faults such as the Kolumbo Fault or the Christiana Fault (Figure 5f) (Preine, Karstens, Hübscher, Crutchley, et al., 2022), which have much lower throws (<100 m). Also, faults observed within the Thera Pyroclastic Formation in the caldera of Santorini have only minor throws (<100 m) (Drymoni et al., 2022).

Recent findings by Acocella and Trippanera (2016) offer potential explanations. These authors suggest that amagmatic faulting becomes essentially hindered by the emplacement of dikes, e.g. in Iceland (Acocella & Trippanera, 2016), the northern Ethiopian rift (Keir et al., 2006), and the Costa Rica rift (Wilson et al., 2019), where a competition between magmatic and tectonic strain accommodation has been identified (Corti et al., 2003). Numerous dikes have been identified at the cliffs of Santorini (Drymoni et al., 2020, 2022) and also inside the crater of Kolumbo (Nomikou et al., 2012), which are roughly NE-SW aligned (Heath et al., 2019). In addition, the presence of the low-velocity body underneath the northern caldera basin and Kolumbo in 3–5 km depth implies that the shallow crust is strongly overprinted by magmatism (Heath et al., 2019; Hooft et al., 2019; McVey et al., 2020; Schmid et al., 2022). The numerous occurrence of magmatic intrusions combined with the concept by Acocella and Trippanera (2016) may suggest that magmatism has accommodated much of the local strain along the proto Anhydros Basin, while the non-volcanic basins accommodated strain by extensive hanging-wall rotation and internal deformation.

Considering that the early volcanic centers of Kolumbo and Poseidon aligned parallel to the NE-SW directed fault trend in Early Pleistocene, magmatic intrusions have likely been abundant along the deeper subsurface throughout the CSK rift zone since the onset of extensive NE-SW directed faulting in Early Pleistocene. An example of the presence of shallow intrusions is the saucer-shaped reflection underneath the Kolumbo Volcanic Chain in Profile A (Figure 2a), which is an indication of sill intrusions (Planke et al., 2005). We propose that the early evolution of large-scale magmatic intrusions since Middle Pleistocene (during deposition of Unit 3) has hindered the formation of extensive marginal faults at Santorini, the western Anhydros Basin, and the Christiana Basin as observed in the other amagmatic basins.

Consequently, our study suggests sensitive volcano-tectonic feedback mechanisms at the CSK rift zone, in which large-scale tectonics seem to have a primary influence both on the evolution of the rift basins and the emplacement of volcanism while, in turn, magmatism seems to have a secondary influence, essentially hindering the evolution of large-scale faults along the CSK volcanic field.

5.4. Implications for the Evolution of the Hellenic Arc

While reconstructions of the tectonic evolution of the Hellenic Arc have been presented on broad time scales since Oligocene (e.g., Jolivet & Brun, 2010; Jolivet & Faccenna, 2000; Jolivet et al., 2013; Royden & Papanikolaou, 2011), detailed studies of the tectonic and volcanic evolution of the Arc during the last ∼4 Million years are missing so far. However, a few regional studies are available, which enable a qualitative comparison of broader volcano-tectonic changes along the Hellenic Arc since the Pliocene.

Since the volcano-tectonic evolution can be subdivided into distinct phases, it is unclear whether these relate to the local manifestation of the evolving stress regime or to general trends affecting the entire Hellenic Arc. As a proxy for the general tectonic evolution of the eastern Hellenic Arc, Van Hinsbergen et al. (2007) investigated the Plio-Pleistocene tectonic history of the island of Rhodos in the southeastern Aegean Sea (Figure 6) and identified four major tectonic episodes. The first episode occurred between 3.8 and 3.6 Ma and led to a $9 \pm 6°$ counterclockwise rotation of Rhodos (Figure 6a). A second episode occurred between 2.5 and 1.8 Ma tilting Rhodos to the SE while between 1.5 and 1.1 Ma Rhodos tilted to the NW (Figure 6a). The last tectonic phase started at approx. 0.8 Ma when counterclockwise rotation initiated again (Figure 6a). Counterclockwise rotation also affected the western margin of the Rhodos Basin as shown by seismic studies (Figure 6b) (Hall et al., 2009) and has generally been suggested to be the result of the increasing curvature of the Hellenic Arc (ten Veen & Kleinspehn, 2002). Figure 6a shows that the ages of the tectonic events on Rhodos correspond to those of several major unconformities of the CSK rift.

The first counterclockwise rotation event of Rhodes corresponds roughly to the age of unconformity h2 (∼3.4 Ma), i.e., the transition from E-W to NE-SW directed extension (Figure 6). The initiation of the second episode of counterclockwise rotation on Rhodes occurred approx. simultaneously to the first tectonic pulse of the CSK rift (∼0.7 Ma) indicating that these events represent large-scale tectonic reorganizations affecting the entire southeastern Aegean. Figure 6a also shows that both tilting episodes on Rhodos occurred approx. simultaneously to the volcanic activity of Christiana as well as the activity of the Poseidon center and early Kolumbo, suggesting an influence of the arc-wide tectonic regime on the volcanism of the Hellenic Arc. This hypothesis is further supported by comparing the evolution of the CSK volcanic field with that of the Kos-Nisyros-Yali complex on the eastern Hellenic Volcanic Arc (Figure 6). The earliest volcanic activity of the Kos-Nisyros-Yali volcanic complex built dome complexes on southern Kos between 3.4 and 1.6 Ma (e.g., Vougioukalakis et al., 2019) approx. during the same time as Christiana was active and Rhodos tilted first (Figure 6a). Subsequently, volcanic activity became more explosive as demonstrated by the Kefalos Tuff ring that was formed about 0.5 Ma and by the 0.161 ka Kos Plateau Tuff eruption representing one of the largest known explosive eruptions of the Hellenic Arc, which involved a major caldera collapse south of Kos (e.g., Allen & Cas, 2001; Bachmann et al., 2010). Within the last 100 ka, there were at least two major eruptions with estimated tephra volumes exceeding 10 km^3 (Nisyros 1 and Yali 2; Kutterolf et al., 2021).

The similar NE-SW orientation of volcanic and tectonic structures of the Kos-Nisyros-Yali complex (e.g., Nomikou & Papanikolaou, 2011; Nomikou, Papanikolaou, & Dietrich, 2018; Nomikou et al., 2013; Papanikolaou & Nomikou, 2001; Tibaldi et al., 2008) and the CSK field, as well as the general trend from largely effusive volcanism in Late Pliocene/Early Pleistocene toward highly explosive volcanism in Late Pleistocene, highlights volcano-tectonic similarities of both systems (Figure 6a). In addition, Figure 6 shows that discrete phases of counterclockwise rotation and tilting at Rhodos correspond not only to distinct phases of volcanism at the CSK field but also at the Kos-Nisyros-Yali complex indicating regional-scale volcano-tectonic feedback links. Similar to the observations of Flaherty et al. (2022) of a distinct change of primitive melt chemistry after the tectonic pulse at ∼0.36 Ma at the CSK field, each of the previous large-scale tectonic episodes may have influenced the stress in the deeper crust of the broader southeastern Aegean changing fluxes as well as proportions of primitive melts from deep magma reservoirs. Such large-scale volcano-tectonic feedback links have hardly been explored so far and the Hellenic Arc offers the opportunity to derive a spatio-temporal reconstruction of an entire Arc System. However, systematic seismic studies are required for this, which are lacking for most parts of the southern Aegean Sea. This is needed to gain a more holistic understanding of volcano-tectonic processes at an arc scale and to improve hazard assessments of the densely populated pan-Aegean realm.

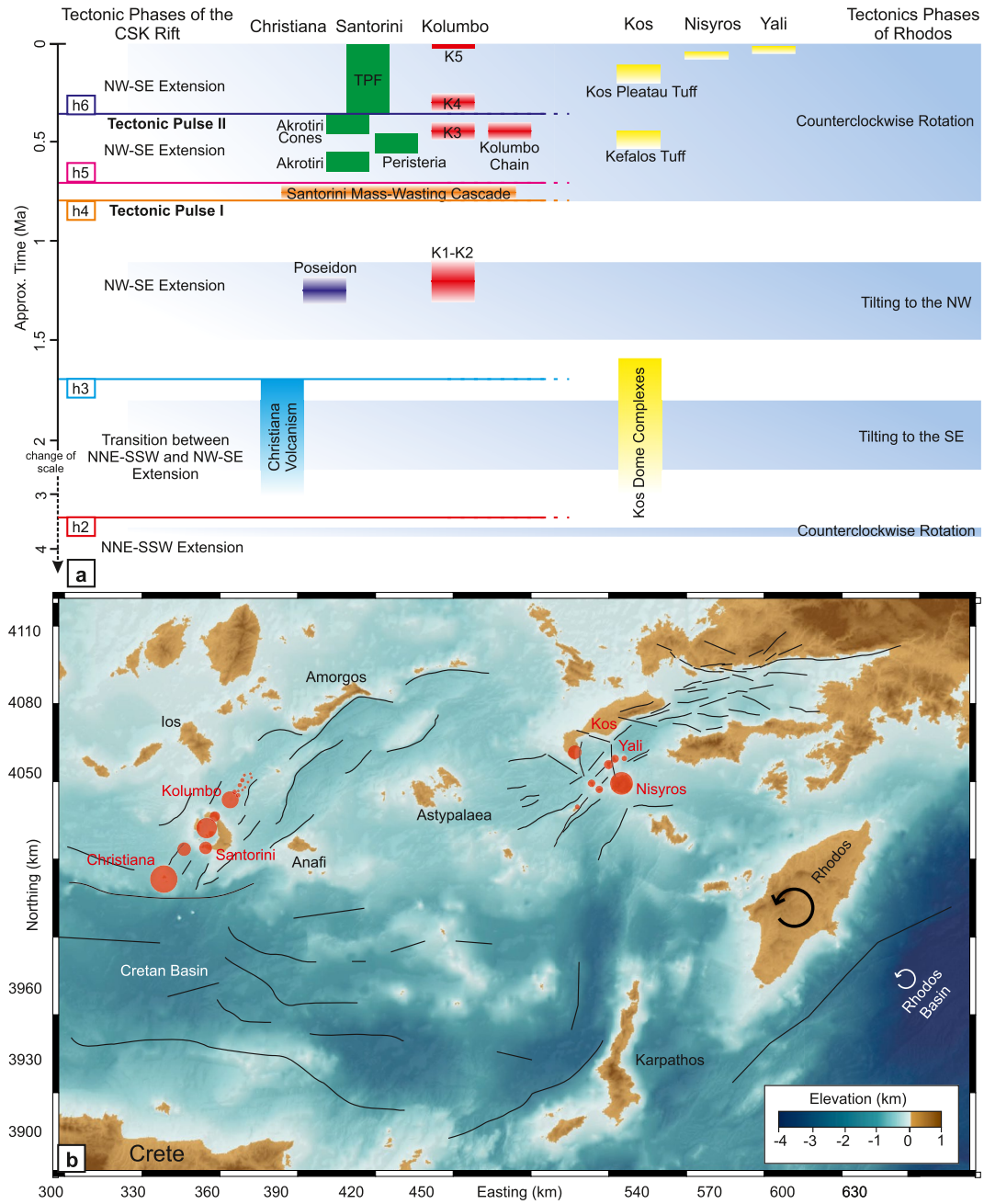

Figure 6. (a) Schematic illustration of the chronology of volcanism and tectonics of the southeastern Aegean Sea. Tectonic phases of the CSK rift are from this study, volcanic ages of the CSK volcanic field from Preine, Karstens, Hübscher, Nomikou, et al. (2022), volcanic ages of the Kos-Nisyros-Yali Complex from Vougioukalakis et al. (2019) as well as Kutterolf et al. (2021), and tectonic phases of Rhodos from Van Hinsbergen et al. (2007). (b) Morphological map of the southeastern Aegean Sea with volcanic centers marked in red. Major tectonic lines of the CSK field and the Kos-Nisyros-Yali complex are marked in black and have been modified from Nomikou et al. (2013); Nomikou, Hübscher, et al. (2018); Nomikou, Papanikolaou, & Dietrich, (2018), and Preine, Karstens, Hübscher, Crutchley, et al. (2022). Additional faults have been modified from Ganas et al. (2013).

6. Conclusions

In this study, we have for the first time consistently linked the evolution of the volcanoes of the Christiana-Santorini-Kolumbo (CSK) volcanic field to the tectonic evolution of the hosting rift basins. Our study shows that distinct volcanic phases correlate with major changes in the tectonic behavior of the rift system.

According to our interpretation, a Pliocene NNE-SSW-directed proto basin existed underneath Kolumbo, the Kolumbo volcanic chain, and continued underneath Santorini towards Christiana. This basin acted as a transfer zone between WNW-ESE-oriented Pliocene basins. Volcanism initiated with the onset of NW-SE-directed rifting, which became the main orientation of the emplacement of volcanic edifices in the Pleistocene. Distinct tectonic pulses preceded major changes in the volcanic evolution of the CSK volcanic field. A major rift pulse at approx. 0.7 Ma triggered large-scale mass wasting events, which initiated the emergence of widespread volcanism. Another large-scale tectonic pulse occurred at approx. 0.36 Ma, which corresponds to a distinct shift of Santorini's volcanism marking the transition from effusive to highly explosive eruptions. This transition also corresponds to a change in primitive melt chemistry at Santorini implying deep-seated feedback mechanisms between the regional tectonic regime and the volcanic plumbing system of the CSK field.

We argue that the incremental tectonic reorganizations of the rift might be related to the increasing curvature of the Hellenic Arc that induced counterclockwise rotation and enhanced internal deformation along the entire southeastern Aegean. Vice-versa, our analysis indicates that magmatism at the CSK volcanic field might have hindered the formation of major marginal faults along the CSK volcanic field, which define the morphology of the non-volcanic basins of the rift system. Consequently, the CSK volcanic field reveals volcano-tectonic feedback links in which regional tectonics seem to have had a primary influence on both basin evolution and emplacement of volcanoes, while subsequent magmatism seems to have had a secondary influence on the tectonic system by accommodating extensional strain in the volcanic basins. Understanding such volcano-tectonic feedback mechanisms is critical to improving future hazard assessments for the Aegean and we strongly encourage similar seismic studies to be conducted for the neighboring volcanic centers of the Hellenic Arc to reconstruct their volcano-tectonic evolution.

Data Availability Statement

SEG-Y files of the seismic lines shown in Figure 2 are available in the Marine Geoscience Data System with data https://doi.org/10.26022/IEDA/331028.

Acknowledgments
The authors would like to thank the captains, crews, and scientific parties of RV Poseidon POS538 and POS338 expeditions and RV Aegeo THERA expedition. We kindly thank Rebecca Bell and Dave Tappin for improving the quality of this manuscript. Tim Druitt and Gareth Crutchley are thanked for helpful discussions. The authors thankfully acknowledge the support of the German Research Foundation DFG (HU690/25-1). In addition, the authors are grateful to Schlumberger for providing VISTA seismic processing software and IHS Markit for providing KINGDOM seismic interpretation software. Open Access funding enabled and organized by Projekt DEAL.

References

Acocella, V. (2021). Volcano-Tectonic Processes. In *Volcano-Tectonic Processes*. Springer Nature. https://doi.org/10.1007/978-3-030-65968-4

Acocella, V., & Trippanera, D. (2016). How diking affects the tectonomagmatic evolution of slow spreading plate boundaries: Overview and model. *Geosphere*, *12*(3), 867–883. https://doi.org/10.1130/ges01271.1

Allen, S. R., & Cas, R. A. (2001). Transport of pyroclastic flows across the sea during the explosive, rhyolitic eruption of the Kos Plateau Tuff, Greece. *Bulletin of Volcanology*, *62*(6), 441–456. https://doi.org/10.1007/s004450000107

Anastasakis, G., & Piper, D. J. (2005). Late Neogene evolution of the western South Aegean volcanic arc: Sedimentary imprint of volcanicity around Milos. *Marine Geology*, *215*, 135–158. https://doi.org/10.1016/j.margeo.2004.11.014

Bachmann, O., Schoene, B., Schnyder, C., & Spikings, R. (2010). The 40Ar/39Ar and U/Pb dating of young rhyolites in the Kos-Nisyros volcanic complex, Eastern Aegean Arc, Greece: Age discordance due to excess 40Ar in biotite. *Geochemistry, Geophysics, Geosystems*, *11*(8). https://doi.org/10.1029/2010GC003073

Bocchini, G. M., Brüstle, A., Becker, D., Meier, T., Van Keken, P. E., Ruscic, M., et al. (2018). Tearing, segmentation, and backstepping of subduction in the Aegean: New insights from seismicity. *Tectonophysics*, *734*, 96–118. https://doi.org/10.1016/j.tecto.2018.04.002

Bohnhoff, M., Rische, M., Meier, T., Becker, D., Stavrakakis, G., & Harjes, H. P. (2006). Microseismic activity in the Hellenic Volcanic Arc, Greece, with emphasis on the seismotectonic setting of the Santorini–Amorgos zone. *Tectonophysics*, *423*(1–4), 17–33. https://doi.org/10.1016/j.tecto.2006.03.024

Brüstle, A., Friederich, W., Meier, T., & Gross, C. (2014). Focal mechanism and depth of the 1956 Amorgos twin earthquakes from waveform matching of analogue seismograms. *Solid Earth*, *5*(2), 1027–1044. https://doi.org/10.5194/se-5-1027-2014

Corti, G., Bonini, M., Conticelli, S., Innocenti, F., Manetti, P., & Sokoutis, D. (2003). Analogue modelling of continental extension: A review focused on the relations between the patterns of deformation and the presence of magma. *Earth-Science Reviews*, *63*(3–4), 169–247. https://doi.org/10.1016/S0012-8252(03)00035-7

Druitt, T. H., Edwards, L., Mellors, R. M., Pyle, D. M., Sparks, R. S. J., Lanphere, M., et al. (1999). *Santorini volcano* (p. 19). Geological Society Memoir.

Druitt, T. H., McCoy, F. W., & Vougioukalakis, G. E. (2019). The Late Bronze Age eruption of Santorini volcano and its impact on the ancient Mediterranean world. *Elements*, *15*(3), 185–190. https://doi.org/10.2138/gselements.15.3.185

Drymoni, K., Browning, J., & Gudmundsson, A. (2020). Dyke-arrest scenarios in extensional regimes: Insights from field observations and numerical models, Santorini, Greece. *Journal of Volcanology and Geothermal Research*, *396*, 106854. https://doi.org/10.1016/j.jvolgeores.2020.106854

Drymoni, K., Browning, J., & Gudmundsson, A. (2022). Spatial and temporal volcanotectonic evolution of Santorini volcano, Greece. *Bulletin of Volcanology*, *84*(6), 1–18. https://doi.org/10.1016/10.1007/s00445-022-01566-4

Faulds, J. E., & Varga, R. J. (1998). The role of accommodation zones and transfer zones in the regional segmentation of extended terranes. *Geological Society of America Special Paper*, *323*, 1–45. https://doi.org/10.1130/0-8137-2323-X.1

Flaherty, T., Druitt, T. H., Francalanci, L., Schiano, P., & Sigmarsson, O. (2022). Temporal variations in the diversity of primitive melts supplied to the Santorini silicic magmatic system and links to lithospheric stresses. *Contributions to Mineralogy and Petrology*, *177*, 79. https://doi.org/10.1007/s00410-022-01941-6

Ganas, A., Oikonomou, I. A., & Tsimi, C. (2013). NOAFAULTS: A digital database for active faults in Greece in bulletin of the geological society of Greece, v. XLVII. In *Proceedings of the 13th International Cogfress, Chania*.

Gautier, P., Brun, J. P., Moriceau, R., Sokoutis, D., Martinod, J., & Jolivet, L. (1999). Timing, kinematics and cause of Aegean extension: A scenario based on a comparison with simple analogue experiments. *Tectonophysics*, *315*(1–4), 31–72. https://doi.org/10.1016/S0040-1951(99)00281-4

Giba, M., Walsh, J. J., Nicol, A., Mouslopoulou, V., & Seebeck, H. (2013). Investigation of the spatio-temporal relationship between normal faulting and arc volcanism on million-year time scales. *Journal of the Geological Society*, *170*(6), 951–962. https://doi.org/10.1144/jgs2012-121

Hall, J., Aksu, A. E., Yaltırak, C., & Winsor, J. D. (2009). Structural architecture of the Rhodes Basin: A deep depocentre that evolved since the Pliocene at the junction of Hellenic and Cyprus Arcs, eastern Mediterranean. *Marine Geology*, *258*(1–4), 1–23. https://doi.org/10.1016/j.margeo.2008.02.007

Heath, B. A., Hooft, E. E. E., Toomey, D. R., Papazachos, C. B., Nomikou, P., Paulatto, M., et al. (2019). Tectonism and its relation to magmatism around Santorini Volcano from upper crustal P wave velocity. *Journal of Geophysical Research: Solid Earth*, *124*, 10610–10629. https://doi.org/10.1029/2019JB017699

Heath, B. A., Hooft, E. E. E., Toomey, D. R., Paulatto, M., Papazachos, C. B., Nomikou, P., & Morgan, J. V. (2021). Relationship between active faulting/fracturing and magmatism around Santorini: Seismic anisotropy from an active source tomography experiment. *Journal of Geophysical Research: Solid Earth*, *126*. https://doi.org/10.1029/2021JB021898

Hill, D. P., Pollitz, F., & Newhall, C. (2002). Earthquake-volcano interactions. *Physics Today*, *55*, 41–47. https://doi.org/10.1063/1.1535006

Hooft, E. E., Nomikou, P., Toomey, D. R., Lampridou, D., Getz, C., Christopoulou, M. E., et al. (2017). Backarc tectonism, volcanism, and mass wasting shape seafloor morphology in the Santorini-Christiana-Amorgos region of the Hellenic Volcanic Arc. *Tectonophysics*, *712*, 396–414. https://doi.org/10.1016/j.tecto.2017.06.005

Hooft, E. E. E., Heath, B. A., Toomey, D. R., Paulatto, M., Papazachos, C. B., Nomikou, P., et al. (2019). Seismic imaging of Santorini: Subsurface constraints on caldera collapse and present-day magma recharge. *Earth and Planetary Science Letters*, *514*, 48–61. https://doi.org/10.1016/j.epsl.2019.02.033

Hübscher, C., Hensch, M., Dahm, T., Dehghani, A., Dimitriadis, I., Hort, M., & Taymaz, T. (2006). Toward a risk assessment of central Aegean volcanoes. *Eos, Transactions American Geophysical Union*, *87*(39), 401–407. https://doi.org/10.1029/2006EO390002

Hübscher, C., Ruhnau, M., & Nomikou, P. (2015). Volcano-tectonic evolution of the polygenetic Kolumbo submarine volcano/Santorini (Aegean Sea). *Journal of Volcanology and Geothermal Research*, *291*, 101–111. https://doi.org/10.1016/j.jvolgeores.2014.12.020

Jamaludin, S. F., Latiff, A. A., & Ghosh, D. P. (2015). Structural balancing vs horizon flattening on seismic data: Example from extensional tectonic setting. In *IOP Conference Series: Earth and Environmental Science*. IOP Publishing. https://doi.org/10.1088/1755-1315/23/1/012003

Johnston, E. N., Sparks, R. S. J., Phillips, J. C., & Carey, S. (2014). Revised estimates for the volume of the Late Bronze Age Minoan eruption, Santorini, Greece. *Journal of the Geological Society*, *171*(4), 583–590. https://doi.org/10.1144/jgs2013-113

Jolivet, L. (2001). A comparison of geodetic and finite strain pattern in the Aegean, geodynamic implications. *Earth and Planetary Science Letters*, *187*(1–2), 95–104. https://doi.org/10.1016/S0012-821X(01)00277-1

Jolivet, L., & Brun, J. P. (2010). Cenozoic geodynamic evolution of the Aegean. *International Journal of Earth Sciences*, *99*(1), 109–138. https://doi.org/10.1007/s00531-008-0366-4

Jolivet, L., & Faccenna, C. (2000). Mediterranean extension and the Africa-Eurasia collision. *Tectonics*, *19*(6), 1095–1106. https://doi.org/10.1029/2000TC900018

Jolivet, L., Faccenna, C., Huet, B., Labrousse, L., Le Pourhiet, L., & Lacombe, O. (2013). Aegean tectonics: Strain localisation, slab tearing and trench retreat. *Tectonophysics*, *597*, 1–33. https://doi.org/10.1016/j.tecto.2012.06.011

Karstens, J., Crutchley, G., Elger, J., Kühn, M., Schmid, F., Dalla Valle, G., et al. (2020). R/V Poseidon Cruise Report 538-THESEUS Tsunami hazard of explosive submarine eruptions, 15th July–26th July, 2019 Cartagena (Spain)-Heraklion (Greece). Retrieved from http://oceanrep.geomar.de/id/eprint/49501

Keir, D., Ebinger, C. J., Stuart, G. W., Daly, E., & Ayele, A. (2006). Strain accommodation by magmatism and faulting as rifting proceeds to breakup: Seismicity of the northern Ethiopian rift. *Journal of Geophysical Research*, *111*(B5). https://doi.org/10.1029/2005JB003748

Kutterolf, S., Freundt, A., Druitt, T. H., McPhie, J., Nomikou, P., Pank, K., et al. (2021). The medial offshore record of explosive volcanism along the central to eastern Aegean Volcanic Arc: 2. Tephra ages and volumes, eruption magnitudes and marine sedimentation rate variations. *Geochemistry, Geophysics, Geosystems*, *22*(12). https://doi.org/10.1029/2021GC010011

Le Pichon, X., & Angelier, J. (1979). The Hellenic Arc and trench system: A key to the neotectonic evolution of the eastern Mediterranean area. *Tectonophysics*, *60*(1–2), 1–42. https://doi.org/10.1016/0040-1951(79)90131-8

Le Pichon, X., & Kreemer, C. (2010). The Miocene-to-present kinematic evolution of the Eastern Mediterranean and Middle East and its implications for dynamics. *Annual Review of Earth and Planetary Sciences*, *38*, 323–351. https://doi.org/10.1146/annurev-earth-040809-152419

Lisiecki, L. E., & Raymo, M. E. (2005). A Pliocene-Pleistocene stack of 57 globally distributed benthic δ18O records. *Paleoceanography*, *20*(1), a–n. https://doi.org/10.1029/2004PA001071

Manga, M., & Brodsky, E. (2006). Seismic triggering of eruptions in the far field: Volcanoes and geysers. *Annual Review of Earth and Planetary Sciences*, *34*, 263–291. https://doi.org/10.1146/annurev.earth.34.031405.125125

McVey, B. G., Hooft, E. E. E., Heath, B. A., Toomey, D. R., Paulatto, M., Morgan, J. V., et al. (2020). Magma accumulation beneath Santorini volcano, Greece, from P-wave tomography. *Geology*, *48*(3), 231–235. https://doi.org/10.1130/G47127.1

Nomikou, P., Carey, S., Papanikolaou, D., Bell, K. C., Sakellariou, D., Alexandri, M., & Bejelou, K. (2012). Submarine volcanoes of the Kolumbo volcanic zone NE of Santorini Caldera, Greece. *Global and Planetary Change*, *90*, 135–151. https://doi.org/10.1016/j.gloplacha.2012.01.001

Nomikou, P., Druitt, T. H., Hübscher, C., Mather, T. A., Paulatto, M., Kalnins, L. M., et al. (2016a). Post-eruptive flooding of Santorini caldera and implications for tsunami generation. *Nature Communications*, *7*(1), 1–10. https://doi.org/10.1038/ncomms13332

Nomikou, P., Hübscher, C., & Carey, S. (2019). The Christiana–Santorini–Kolumbo Volcanic Field. *Elements: An International Magazine of Mineralogy, Geochemistry, and Petrology*, *15*(3), 171–176. https://doi.org/10.2138/gselements.15.3.171

Nomikou, P., Hübscher, C., Papanikolaou, D., Farangitakis, G. P., Ruhnau, M., & Lampridou, D. (2018). Expanding extension, subsidence and lateral segmentation within the Santorini-Amorgos basins during Quaternary: Implications for the 1956 Amorgos events, central-south Aegean Sea, Greece. *Tectonophysics*, *722*, 138–153. https://doi.org/10.1016/j.tecto.2017.10.016

Nomikou, P., Hübscher, C., Ruhnau, M., & Bejelou, K. (2016b). Tectono-stratigraphic evolution through successive extensional events of the Anydros Basin, hosting Kolumbo volcanic field at the Aegean Sea, Greece. *Tectonophysics*, *671*, 202–217. https://doi.org/10.1016/j.tecto.2016.01.021

Nomikou, P., & Papanikolaou, D. (2011). Extension of active fault zones on Nisyros volcano across the Yali-Nisyros Channel based on onshore and offshore data. *Marine Geophysical Research*, *32*(1), 181. https://doi.org/10.1007/s11001-011-9119-z

Nomikou, P., Papanikolaou, D., Alexandri, M., Sakellariou, D., & Rousakis, G. (2013). Submarine volcanoes along the Aegean volcanic arc. *Tectonophysics*, *597*, 123–146. https://doi.org/10.1016/j.tecto.2012.10.001

Nomikou, P., Papanikolaou, D., & Dietrich, V. J. (2018). Geodynamics and volcanism in the Kos-Yali-Nisyros volcanic field. In *Nisyros Volcano* (pp. 13–55). Springer. https://doi.org/10.1007/978-3-319-55460-0_2

Nunns, A. G. (1991). Structural restoration of seismic and geologic sections in extensional regimes. *AAPG Bulletin*, *75*(2), 278–297. https://doi.org/10.1306/0C9B27A9-1710-11D7-8645000102C1865D

Okal, E. A., Synolakis, C. E., Uslu, B., Kalligeris, N., & Voukouvalas, E. (2009). The 1956 earthquake and tsunami in Amorgos, Greece. *Geophysical Journal International*, *178*(3), 1533–1554. https://doi.org/10.1111/j.1365-246X.2009.04237.x

Papanikolaou, D., & Nomikou, P. (2001). Tectonic structure and volcanic centers at the eastern edge of the Aegean volcanic arc around Nisyros island. *Bulletin of the Geological Society of Greece*, *34*(1), 289–296. https://doi.org/10.12681/bgsg.17025

Papazachos, C. B. (2019). Deep structure and active tectonics of the South Aegean volcanic arc. *Elements: An International Magazine of Mineralogy, Geochemistry, and Petrology*, *15*(3), 153–158. https://doi.org/10.2138/gselements.15.3.153

Pe-Piper, G., & Piper, D. J. (2007). Neogene backarc volcanism of the Aegean: New insights into the relationship between magmatism and tectonics. *Special Papers - Geological Society of America*, *418*, 17. https://doi.org/10.1130/2007.2418(02)

Perissoratis, C. (1995). The Santorini volcanic complex and its relation to the stratigraphy and structure of the Aegean arc, Greece. *Marine Geology*, *128*(1–2), 37–58. https://doi.org/10.1016/0025-3227(95)00090-L

Piper, D. J. W., Pe-Piper, G., Perissoratis, C., & Anastasakis, G. (2007). Distribution and chronology of submarine volcanic rocks around Santorini and their relationship to faulting. *Geological Society, London, Special Publications*, *291*(1), 99–111. https://doi.org/10.1144/SP291.5

Piper, D. J. W., & Perissoratis, C. (2003). Quaternary neotectonics of the South Aegean arc. *Marine Geology*, *198*(3–4), 259–288. https://doi.org/10.1016/S0025-3227(03)00118-X

Planke, S., Rasmussen, T., Rey, S. S., & Myklebust, R. (2005). Seismic characteristics and distribution of volcanic intrusions and hydrothermal vent complexes in the Vøring and Møre basins. *Geological Society, London, Petroleum Geology Conference series* (Vol. 6, pp. 833–844). Geological Society of London. https://doi.org/10.1144/0060833

Preine, J., Karstens, J., Hübscher, C., Crutchley, G. J., Druitt, T. H., Schmid, F., & Nomikou, P. (2022). The Hidden Giant: How a rift pulse triggered a cascade of sector collapses and voluminous secondary mass-transport events in the early evolution of Santorini. *Basin Research*, *34*, 1465–1485. https://doi.org/10.1111/bre.12667

Preine, J., Karstens, J., Hübscher, C., Nomikou, P., Schmid, F., Crutchley, G., et al. (2022). Spatio-Temporal Evolution of the Christiana-Santorini-Kolumbo Volcanic Field, Aegean Sea. *Geology*, *50*, 96–100. https://doi.org/10.1130/G49167.1

Preine, J., Schwarz, B., Bauer, A., & Hübscher, C. (2020). When there is no offset: A demonstration of seismic diffraction imaging and depth-velocity model building in the southern Aegean Sea. *Journal of Geophysical Research: Solid Earth*, *125*. https://doi.org/10.1029/2020JB019961

Royden, L. H., & Papanikolaou, D. J. (2011). Slab segmentation and late Cenozoic disruption of the Hellenic arc. *Geochemistry, Geophysics, Geosystems*, *12*(3). https://doi.org/10.1029/2010GC003280

Schmid, F., Petersen, G., Hooft, E., Paulatto, M., Chrapkiewicz, K., Hensch, M., & Dahm, T. (2022). Heralds of future volcanism: Swarms of microseismicity beneath the submarine Kolumbo volcano indicate opening of near-vertical fractures exploited by ascending melts. *Geochemistry, Geophysics, Geosystems*, *23*, e2022GC010420. https://doi.org/10.1029/2022GC010420

Sigurdsson, H., Carey, S., Alexandri, M., Vougioukalakis, G., Croff, K., Roman, C., et al. (2006). Marine investigations of Greece's Santorini volcanic field. *Eos, Transactions American Geophysical Union*, *87*(34), 337–342. https://doi.org/10.1029/2006EO340001

Taymaz, T., Jackson, J., & McKenzie, D. (1991). Active tectonics of the north and central Aegean Sea. *Geophysical Journal International*, *106*(2), 433–490. https://doi.org/10.1111/j.1365-246X.1991.tb03906.x

ten Veen, J. H., & Kleinspehn, K. L. (2002). Geodynamics along an increasingly curved convergent plate margin: Late Miocene-Pleistocene Rhodes, Greece. *Tectonics*, *21*. https://doi.org/10.1029/2001TC001287

Tibaldi, A., Pasquare, F. A., Papanikolaou, D., & Nomikou, P. (2008). Tectonics of Nisyros Island, Greece, by field and offshore data, and analogue modelling. *Journal of Structural Geology*, *30*(12), 1489–1506. https://doi.org/10.1016/j.jsg.2008.08.003

Tsampouraki-Kraounaki, K., & Sakellariou, D. (2018). Seismic stratigraphy and geodynamic evolution of Christiana Basin, South Aegean arc. *Marine Geology*, *399*, 135–147. https://doi.org/10.1016/j.margeo.2018.02.012

Van Hinsbergen, D. J., Krijgsman, W., Langereis, C. G., Cornée, J. J., Duermeijer, C. E., & Van Vugt, N. (2007). Discrete Plio-Pleistocene phases of tilting and counterclockwise rotation in the southeastern Aegean arc (Rhodos, Greece): Early Pliocene formation of the south Aegean left-lateral strike-slip system. *Journal of the Geological Society*, *164*(6), 1133–1144. https://doi.org/10.1144/0016-76492006-061

Van Hinsbergen, D. J., & Schmid, S. M. (2012). Map viewrestoration of Aegean–West Anatolian accretion and extension since the Eocene. *Tectonics*, *31*(5), TC5005. https://doi.org/10.1029/2012TC003132

Vougioukalakis, G. E., Satow, C. G., & Druitt, T. H. (2019). Volcanism of the South Aegean volcanic arc. *Elements: An International Magazine of Mineralogy, Geochemistry, and Petrology*, *15*(3), 159–164. https://doi.org/10.2138/gselements.15.3.159

Watt, S. F., Pyle, D. M., & Mather, T. A. (2009). The influence of great earthquakes on volcanic eruption rate along the Chilean subduction zone. *Earth and Planetary Science Letters*, *277*(3–4), 399–407. https://doi.org/10.1016/j.epsl.2008.11.005

Wilson, D. J., Robinson, A. H., Hobbs, R. W., Peirce, C., & Funnell, M. J. (2019). Does intermediate spreading-rate oceanic crust result from episodic transition between magmatic and magma-dominated, faulting-enhanced spreading?—The Costa Rica Rift example. *Geophysical Journal International*, *218*(3), 1617–1641. https://doi.org/10.1093/gji/ggz184

Zhu, L., Mitchell, B. J., Akyol, N., Cemen, I., & Kekovali, K. (2006). Crustal thickness variations in the Aegean region and implications for the extension of continental crust. *Journal of Geophysical Research*, *111*(B1). https://doi.org/10.1029/2005JB003770